EUROPEAN ORGANISATION FOR NUCLEAR RESEARCH

CERN-PPE/91-32
February 20, 1991

The Trigger System of the OPAL Experiment at LEP

M. Arignon[12], A.H. Ball[9], K.W. Bell[11], M. Bramhall[11], A. Braun[5], A.A. Carter[7], J.R. Carter[3], D.G. Charlton[4], M. Dittmar[2], P. Farthouat[12,a], J. Feyt[4], H. Gao[5], J.W. Gary[6], J.D. Gillies[11], C. Greiner[5], R. Hammarstroem[4], J. Hart[3], R.-D. Heuer[4], J.C. Hill[3], S.J. Hillier[1], T. Hilse[5], R. Humbert[5], S. Jaroslawski[11], D. Joos[5], P. Jovanovic[1], T. Kawamoto[13], R.G. Kellogg[9], T. Kobayashi[13], P. Le Du[12], L.J. Levinson[14], F.K. Loebinger[8], A.A. MacBeth[8], G. Mikenberg[14], R. Milborrow[11], S.J. Pawley[8], A. Penton[11], T.W. Pritchard[7], G. Quast[4], G. Rieth[5], C.M. Roach[3], K. Runge[5], O. Schaile[5], D. Scherer[5], G. Schuler[4], J. Schwarz[5], R.W. Springer[9], H. Takeda[13,b], C.J. Virtue[10], A. Wagner[6], D.R. Ward[3], P.M. Watkins[1], M. Webel[5], C. Weber[5], M. Weymann[4], G.W. Wilson[12], J.A. Wilson[1]

[1]School of Physics and Space Research, University of Birmingham, Birmingham, B15 2TT, UK
[2]Department of Physics, University of California, Riverside, CA 92521 USA
[3]Cavendish Laboratory, Cambridge, CB3 0HE, UK
[4]CERN, European Organisation for Particle Physics, 1211 Geneva 23, Switzerland
[5]Fakultät für Physik, Albert Ludwigs Universität, D-7800 Freiburg, FRG
[6]Physikalisches Institut, Universität Heidelberg, D-6900 Heidelberg, FRG
[7]Queen Mary and Westfield College, University of London, London, E1 4NS, UK
[8]Department of Physics, Schuster Laboratory, The University, Manchester, M13 9PL, UK
[9]Dept. of Physics and Astronomy, University of Maryland, College Park, Maryland 20742, USA
[10]National Research Council, Herzberg Institute of Astrophysics, Ottawa, Ont. K1A 0R6, Canada
[11]Rutherford Appleton Laboratory, Chilton, Didcot, Oxfordshire, OX11 0QX, UK
[12]DPhPE, CEN Saclay, F-91191 Gif-sur-Yvette, France
[13]Int. Center for Elementary Particle Phys. and Dept. of Phys., Univ. of Tokyo, Tokyo 113, Japan
[14]Nuclear Physics Department, Weizmann Institute of Science, Rehovot, 76100, Israel

[a]Present address: CERN, Geneva, Switzerland
[b]Present address: Kobe University, Kobe 657, Japan

Abstract

This paper describes the trigger system of the OPAL detector at the e^+e^- collider LEP and its performance during the first year of data taking. A high level of redundancy and fine detector segmentation at the trigger level led to a high efficiency for all considered physics reactions while the trigger rates were kept low.

(submitted to Nucl. Instr. and Meth.)

1 Introduction

The LEP electron-positron collider, running at centre-of-mass energies around the Z^0 mass, is uniquely placed to make precision tests of the Standard Model. Low background levels allow efficient collection of events over almost the full solid angle. In particular, distinctive physics and background signatures allow strong discrimination to be made at the trigger level. Precise understanding of any residual inefficiencies may be obtained with several independent triggers. The OPAL trigger system, described here, provides a high level of such redundancy, in a single, deadtimeless stage.

The OPAL detector [1] is one of the four large experiments at the e^+e^- collider LEP, at CERN. OPAL is a multipurpose apparatus providing full acceptance for visible Z^0 decays over a solid angle of close to 4π steradians. The general layout of the detector is shown in fig. 1, indicating the location and relative size of the various subdetector components. A system of central tracking chambers is contained inside a solenoid which provides a uniform magnetic field of 0.435 T. The solenoidal coil is surrounded by a time-of-flight counter array, a lead glass electromagnetic calorimeter with a presampler, an instrumented magnet return yoke serving as a hadron calorimeter and four layers of outer muon chambers. A forward detector measures the luminosity. The trigger decision is based on information from most of these detectors – comprising a "track trigger", a time-of-flight trigger, electromagnetic calorimeter and hadron calorimeter triggers as well as muon detector and forward detector triggers.

Performance constraints are placed on the trigger system by the rate of collisions and the output event rate. With four bunches of electrons and positrons circulating in the machine, the LEP bunch-crossing interval is 22 μs. Chamber drift times of up to 8 μs and electronics reset times up to 7 μs leave several microseconds available for sophisticated triggering. The on-resonance Z^0 production rate is 0.7 Hz at the LEP design luminosity of 1.6×10^{31} cm^{-2}s^{-1}. The tolerable trigger rate depends on the readout deadtime associated with accepted events; given a readout deadtime of 20 ms per event, the trigger rate should not exceed 5 Hz in order to keep losses below 10 %.

The main physics processes that must be triggered efficiently are the multihadronic and charged leptonic decays of the Z^0 and small angle Bhabha scattering for the measurement of luminosity. In addition, it is important to be sensitive to other processes: $e^+e^- \rightarrow \nu\bar{\nu}\gamma$ ("single-photon production") for large-angle photons; $e^+e^- \rightarrow \gamma\gamma$; possible new exotic event signatures, *e.g.* from $e^+e^- \rightarrow Z^0H^0$; and energetic two-photon processes $e^+e^- \rightarrow e^+e^-X$. Essential redundancy is obtained by using both independent detector components and coincidences between different components which are sensitive to single particles.

Backgrounds to these processes come mainly from the following sources: single beam particles interacting with residual gas within, or the walls of, the beam-pipe and synchrotron radiation. As well as not originating from the expected interaction region, background events are characterised by low visible energies and track multiplicities. Separation of low-multiplicity collision events from backgrounds can be made at the trigger level by using information on the vertex position along the beam line. In addition to beam-related backgrounds, cosmic rays and detector noise contribute to the trigger rate.

The OPAL trigger is implemented as separated parts – the different subdetector trigger signals are formed independently and are synthesised by the digital "central trigger logic" processor. The subdetector trigger signals divide into two complementary parts: "direct" trigger signals such as total energy or track multiplicities use information from a single detector component and have relatively high thresholds. In order to allow lower thresholds and spatial coincidences between components the detector has been subdivided into θ and ϕ elements ("θ-ϕ matrix"). The θ-ϕ matrix is composed of

overlapping bins in polar and azimuthal angle (denoted θ and ϕ, respectively[1]). The full azimuthal range is covered by twenty-four bins, the polar range by six bins (see tables 1 and 2). The matrix has five "layers" corresponding to the track, time-of-flight, electromagnetic, hadron and muon triggers. The matrix provides spatial correlations of hits within and between subdetector layers. This is shown schematically in fig. 2.

A positive decision, formed in the central trigger logic by a flexible (programmable) combination of the direct and θ-ϕ triggers, initiates digitisation and readout of the event data. Synchronisation signals are carried on custom "trigger bus" cables between the central trigger logic and subdetector readout crates. The readout system has a microprocessor controlled, multi-level tree structure [2] based on the VME standard [3].

Partial online reconstruction of the digitised event allows further rejection of backgrounds. This second level of triggering will be described elsewhere [4].

In the following sections, the subdetector trigger systems and the central trigger logic are described, followed by a discussion of their performance during the data-taking in 1989 and 1990.

2 The Subdetector Trigger Systems

The detector consists of 14 subdetectors, which can be operated independently. Of these, the vertex chamber, the jet chamber, the time-of-flight detector, the electromagnetic barrel and endcap calorimeters, the hadron barrel, endcap and pole-tip calorimeters, the muon barrel and endcap detectors, and the forward detector provide trigger signals.

Most of the electronics is installed outside the detector due to tight space constraints, and is contained in electronics huts placed around the detector. Signals are carried from the front-end electronics at the subdetectors to the electronics huts by typically 40 m of twisted pair or coaxial cable. The distance between the subdetector electronics and the central trigger logic varies between 10 and 130 m in cable length.

In the following sections the subdetectors, their trigger systems and the signals they provide to the central trigger logic are described, together with an overview of thresholds, efficiencies and typical rates. Event triggering is shown schematically in fig. 3, and table 3 summarises all direct trigger input signals provided by the subdetectors.

2.1 Track Trigger

The central tracking system is divided into a precision vertex chamber, a large volume jet chamber and z-chambers. It operates at a pressure of 4 bar and is therefore contained inside a pressure vessel whose cylindrical structure provides mechanical support to the solenoidal coil mounted around it. Information from the vertex chamber and the jet chamber is used in the track trigger to look for charged particle tracks originating from the vertex in both the r-z and the r-ϕ planes.

The vertex chamber [5] is a 1 m long, 470 mm diameter, cylindrical drift chamber. It consists of an inner layer of 36 cells with 12 axial sense wires each and an outer layer of 36 small angle (4°)

[1] The coordinate system is as follows: The origin is at the nominal interaction point. The x axis is horizontal and points towards the centre of LEP, the y axis is approximately vertical, and the z axis is in the e^- beam direction. The polar angle, θ, is measured from the z axis, and the azimuthal angle, ϕ, from the x axis about the z axis.

stereo cells, containing six sense wires each. The axial cells cover a solid angle of 95% of 4π. They provide a precise measurement of position ($\sigma = 50\ \mu$m) in the r-ϕ plane. A coarse measurement of the coordinate along the anode wire (z) is obtained by measuring the time difference between the signals from the two ends of the wire.

The main tracking is performed with the jet chamber [6], a drift chamber ~4 m long and 2 m in radius. The chamber is subdivided into 24 identical sectors, each containing a plane with 159 sense wires. All wires are parallel to the beam direction and the wire planes are radial. The maximum drift distance varies from 3 cm at the innermost sense wire to 25 cm at the outermost wire. In the range $|\cos\theta| < 0.73$, 159 points are measured along each track, and at least 20 points on a track are obtained over a solid angle of 96% of 4π. For each point, true three-dimensional coordinates (r, ϕ, z) are determined from the wire position, the drift time and from a charge division measurement. The charge division method requires the measurement of the integrated charges for each hit at both ends of the signal wire. The ratio of these charges determines z, and their sum is used to calculate the energy loss, dE/dx, of the particle in the chamber gas.

The track trigger [7] uses information from the 12 axial wires of each sector of the vertex chamber and from three groups of 12 adjacent wires at different radii of each jet chamber sector. Signals formed by the vertex chamber and the jet chamber trigger electronics are combined by the track trigger processor, which detects the presence of tracks in any bins of the θ-ϕ matrix and provides various track multiplicity signals. In addition, simple counts of the number of hit wires are provided, and trigger signals depending on the specific ionisation of particles are available from the jet chamber electronics.

Charged tracks are essentially straight lines in the r-z plane (for transverse momenta p_T >250 MeV) in spite of the axial magnetic field. Therefore tracks emanating from a genuine beam-beam vertex ($z = 0$) will have nearly constant values of θ at all points along the track. A histogram of the z/r ($= \cot\theta$) values for hits on such a track will show a narrow peak at some well-defined z/r value, see fig. 4. Due to the magnetic field, tracks can cross sector boundaries, and bin boundaries in z/r can be crossed due to a finite resolution in z. Therefore the histogram contents are overlapped (*i.e.* summed over adjacent sectors and z/r bins), so that these tracks are not missed. The track trigger processor forms 4×24 of such overlapped histograms, one for each of the four groups of 12 wires in each of 24 ϕ sectors. Tracks are identified by looking for coincident peaks from the wire groups in the resulting distributions.

Vertex Chamber Trigger Electronics

A fast z value for each hit in the vertex chamber is obtained from a time difference measurement of signals propagating to each end of an axial sense wire [8]. This is made by using the signal from one end of the wire to initiate the charging of a capacitor. The signal from the other end is delayed by 5 ns to ensure that it arrives after the start signal and is used to halt the capacitor charging. The voltage across the capacitor, which is proportional to the time between the two signals, is then measured using a 6-bit FADC and this z value is stored in RAM. For this measurement to be both precise and stable, an automatic calibration system injects test pulses into the ends of the sense wires between beam crossings and the reference levels of the FADCs are automatically adjusted. The 6-bit z values are converted to 5-bit z/r values, via a look-up table, and then sent to the track trigger processor. Up to the first six hits on any wire in an event can be used by the track trigger processor.

The total number of hits on the axial wires is also compared with a preset threshold and is available as a direct trigger input.

Jet Chamber Trigger Electronics

The logic used to generate z/r values in the jet chamber [9] is shown in fig. 5. The signals from the two ends of an anode wire in the jet chamber are summed and compared with a computer adjustable threshold which corresponds to $\sim 1/10$ of a minimum ionising particle. If the threshold is exceeded, the sum and the signal from one end are integrated for $\sim$200 ns. The sum, $q_1 + q_2$, is applied as the upper reference voltage to a FADC, and the charge from one end, q_1, is fed into its signal input. In this way the FADC performs a division $q_1/(q_1 + q_2)$, which is a direct measure of the z position of the charge deposit [10]. Via a look-up table the 7-bit z value is converted to a 5-bit z/r value which itself serves as the address for a RAM. The data which are stored at this address are a "hit bit" and the sum of the charges obtained from a second FADC. The hit bit is stored for those hits only where the charge deposited does not exceed ten times that of a minimum ionising particle. All hits on a wire resolved outside this 200 ns integration time are used in this way. After the maximum drift time of ~ 5 μs the hit bits are transferred to the track trigger processor.

The jet chamber trigger electronics also counts hits in each of the three "rings" formed by the groups of 12 wires and compares these with preset thresholds, providing three direct trigger inputs.

The charge sensitive triggers are formed by summing the charges stored in the RAMs for each sector and each z/r value for each group of 12 wires. A trigger sensitive to particles depositing charges smaller than a minimum ionising particle is derived by demanding that there be a minimal number of hits (typically four per group of 12 wires), and that the sums be below a programmable threshold in all three groups of a sector. This threshold depends on the number of hits and is different for each z/r value to account for the θ dependence of the track length; it is set just below the expected charge deposited by a minimum ionising particle. A trigger on highly ionising particles is formed from the outputs of the discriminators flagging charges which correspond to more than 10 times that deposited by a minimum ionising particle. It is demanded that 30 (out of the 36) wires in a sector exceed this threshold.

Track Trigger Processor

The track trigger processor logic is housed in three crates. Two of these contain 24 histogramming modules, one per ϕ bin. Each histogrammer (shown schematically in fig. 6) receives z/r values of hits from the three groups of 12 wires in the jet chamber and from one or two vertex chamber sectors. The hits are histogrammed after 5 μs and then overlapped. Overlapping in ϕ is achieved by summing the histograms from two adjacent histogrammers. The z/r bins are overlapped by shifting the histograms by one bin and adding them. Peaks in the distribution, corresponding to track segments, are found by applying thresholds to each z/r bin in the overlapped histograms. If the number of entries in a bin reaches the preset threshold a track flag is set for that z/r bin. The thresholds can be set independently for each z/r bin in each one of the four rings formed by the groups of 12 wires. Coincidences between the track flags of each z/r bin of the jet chamber groups are formed, optionally requiring all, two or only one of the groups. The processor then looks for coincidences between the vertex and jet chamber track flags, using a custom-designed "coincidence chip" [11], leading to 32×24 track decisions, where bins 1 and 32 signify underflows and overflows, *i.e.* unphysical z measurements. This array of 32×24 decisions is then reduced to the standard 6×24 θ-ϕ matrix by combining the z/r bins into the final overlapping θ bins, and it is also transferred to the next stage, the "multiplicity crate".

The multiplicity crate determines the track multiplicity as ≥ 1, ≥ 2, ≥ 3. This is done both for the full θ range and for the barrel region, which is defined by the θ range covered by the third jet chamber ring. These six outputs are sent to the central trigger logic as direct inputs. All signals are available within 13 μs of beam crossing time.

Performance

The track trigger is flexible and all parts of the decision making are programmable. For most of the data taking period, jet chamber rings 1, 2 and 3 were located at wire numbers 9–20 ($|\cos\theta| < 0.96$), 37–48 ($|\cos\theta| < 0.92$), and 97–108 ($|\cos\theta| < 0.81$), respectively. For 1989 running, only the jet chamber inputs were used for decision making, demanding at least two rings in coincidence. In the 1990 run, the vertex chamber inputs were also used. This increased background rejection without deteriorating the efficiency and allowed an extended θ range, $|\cos\theta| < 0.96$. While the hardware allows for up to 30 z/r slices, only 18 were used, leaving some room for increased background rejection in the future by using the full granularity. The number of hits required in a z/r slice for each group of 12 wires was 4 in the vertex chamber, and 4, 5, 6 in jet chamber rings 1, 2, 3, respectively. In the forward direction ($0.92 < |\cos\theta| < 0.96$), where only wires from the first jet chamber ring and the vertex chamber contribute, this requirement was tightened to $\geq$6 hits in the first ring of the jet chamber for better background rejection. For track finding, hits above threshold were required in all geometrically possible rings.

The signals corresponding to $\geq$3 tracks and $\geq$2 barrel tracks were running at rates of ~0.2 Hz, with some background from beam-wall and beam-gas events, and were used for stand-alone decisions. The efficiency to find a single track was measured from $e^+e^- \to \mu^+\mu^-$ events to be 98.5%, the observed inefficiency being mostly due to low-momentum δ-electrons spiralling in the jet chamber and thereby spoiling the charge division measurement.

The ring hit counts, typically running at 100–500 Hz, were used as a veto on beam-gas and beam-wall background within a trigger on single photon events.

2.2 Time-of-Flight Trigger

The time-of-flight (TOF) scintillation counters are located behind the solenoidal coil and in front of the lead glass and cover the barrel region, $|\cos\theta| < 0.82$. Each of the 160 counters is 6.84 m long, has a trapezoidal cross section (45 mm thick, 89 to 91 mm wide), and an attenuation length of about 2.4 m. Light is collected at both ends of each counter via plexiglass light guides glued directly to phototubes. The TOF system is sensitive to charged particles, and in addition, being located behind ~1.8 radiation lengths ($X_\circ$) of material, it has a very high efficiency for the ~80% of photons which convert in front of it.

Trigger signals from the TOF system are generated from mean timers, and require discriminators on both ends of a counter to have fired, within 50 ns of each other and within 50 ns of the arrival time of a relativistic particle from beam interactions. These 160 signals are used to produce 24 overlapping ϕ bins of 36° each (see table 2), covering all the bins θ_2 to θ_5. Three direct trigger signals are also produced:

- the logical OR of the 160 TOF counters. This signal is very sensitive to machine backgrounds, the typical rate being between 10 and 40 Hz.
- multiplicity counting of TOF counters with an adjustable threshold, typically set to two in order to trigger on showers produced by particles traversing the magnet coil. This signal was used, with other signals in anti-coincidence, as a complementary trigger on single photons.
- multiplicity counting of (overlapping) ϕ bins; the threshold is adjustable and was typically set to seven. This signal triggers on events with several widely spread TOF hits and was used in the early running as an efficient stand-alone trigger for multihadronic events.

Electronics

The 160 coincidence signals from the TOF counters are combined into 40 signals, each of which is the logical OR of four adjacent counters, corresponding to a $\sim 9^\circ$ region in ϕ. These signals are mixed in CAMAC modules to form the 24 overlapping ϕ bins (see table 2). The outputs are shaped to about 1 μs and are sent to the central trigger logic. A majority module builds the OR and the multiplicity counts from the ϕ signals. The 160 coincidence signals are also combined into five groups of 32 and for each group the number of active signals is counted. The five partial sums are added and compared with a preset threshold, providing the TOF counter multiplicity.

Performance

The efficiency of the TOF coincidence signals for single 45 GeV muons was measured to be $97.4 \pm 0.3\%$, when the muon trajectory is fiducially contained within a single counter. It varies from nearly 100% at the centres of the counters to 93% at the ends. The geometrical acceptance (within the nominal solid angle of the TOF system) was found to be $98.0 \pm 0.2\%$, in good agreement with the expected inefficiency caused by the 0.8 mrad azimuthal gaps between counters.

2.3 Electromagnetic Calorimeter Trigger

The electromagnetic calorimeter detects and measures the energies and positions of electrons, positrons and photons ranging from tens of MeV to 100 GeV. It is a hermetic total absorption calorimeter, and is mounted between the coil and the iron yoke of the magnet, as shown in fig. 1. It consists in the barrel region of a cylindrical array of 9,440 lead glass blocks of 24.6 $X_\circ$ thickness, covering $|\cos\theta| < 0.82$, and in the endcaps of 2,264 lead glass blocks of 20 $X_\circ$ thickness, covering $0.81 < |\cos\theta| < 0.98$. This material corresponds to ~ 2 hadronic interaction lengths. There is therefore a high probability of hadronic interactions being initiated in the material of the electromagnetic calorimeter, thus trigger signals from the electromagnetic calorimeter also provide good sensitivity to purely hadronic energy.

In the barrel region, the longitudinal axes of the lead glass blocks point towards the interaction region, to minimise the probability of a particle traversing more than one block. In the z direction, the calorimeter is segmented into 59 blocks, and in the ϕ direction the calorimeter is segmented equally into 160 blocks. Mechanically, the calorimeter is divided into 10 half-ring structures. Each half-ring contains 80 identical ϕ segment modules of 12 lead glass counters (11 for the middle ring). The calorimeter is instrumented with magnetic field tolerant phototubes.

In the endcaps [12], the lead glass blocks are mounted with their axes parallel to the beam line. The front faces of the blocks are arranged to follow the contours of the pressure bell of the central tracking system. The blocks give a total depth of at least 20.5 $X_\circ$ (typically 22 $X_\circ$) for all particles emerging from the interaction region. The calorimeter is instrumented with single stage multipliers known as vacuum photo triodes [13], plus high gain amplifiers.

The trigger logic for the electromagnetic calorimeter is as follows. Several analogue energy sums are provided for different segmentations of the electromagnetic calorimeter, *i.e.* sums over the total barrel, over each endcap, and over each of the 144 θ-ϕ cells. Each energy sum is discriminated at two thresholds, a "high" and a "low". The θ-ϕ segmentation is summarised in tables 1 and 2. The 24-fold fully overlapped ϕ segmentation of the θ-ϕ cells matches as closely as possible that of the track trigger. The θ segmentation arises naturally from the mechanical segmentation of the electromagnetic calorimeter itself. There are two endcaps and five pairs of barrel half-rings, giving seven raw θ segments. Analogue signals from adjacent raw θ segments at the same ϕ are summed to provide the final six-fold overlapping θ segmentation. Each θ-ϕ bin comprises of the analogue sum of 279, 384 or 368 counters (for θ_1, θ_6, θ_2, θ_5, and θ_3, θ_4 respectively).

Implementation

The raw signals from the barrel and endcap counters are digitised by 96-channel charge integrating FASTBUS ADCs [14]. The contribution of each lead glass counter to the trigger is equalised by ensuring that the integrated charges within the ADC gate for each counter for a given amount of deposited electromagnetic energy is the same. This was achieved before first beam in LEP, by adjusting the high voltages of the barrel counters and attenuation resistors of the endcap counters, as part of their calibration in an electron beam. The ADC modules are also equipped with analogue summing circuits. The sum of the integrated charges from 12 consecutive channels, corresponding to a group of 12 neighbouring lead glass counters, is provided as a DC current output. In a next step, the currents of four adjacent outputs are added to form analogue sums of 48 input channels. The electromagnetic triggers are based on these analogue sum signals. There are 200 such signals from the barrel and 24 from each endcap. The sensitivity is 0.1 mA/pC, or equivalently 1 mA/GeV calorimetric energy. The offset voltages of the analogue sum signals are compensated by programmable DACs at the summing circuits. The signal is stable $\sim$4 μs after the ADC gate (of width 720 ns and 1000 ns in the barrel and endcaps, respectively).

The analogue sum signals are then combined in FASTBUS summing modules [15] to form the θ-ϕ signals and the total energy sums of the barrel and each endcap. Each summing module has 40 analogue inputs and 32 outputs, each output being the analogue sum over a number of input signals, individually defined by a resistor network. Programmable DC offset compensation of each analogue sum is provided. Each module has unit gain, and its outputs are compatible with its inputs, allowing them to be used in cascade. For each output channel, there are two discriminators with programmable thresholds. The discrimination is performed $\sim$7 μs after the ADC gate.

Signals to Central Trigger Logic

As well as the discriminated signals from the 144 θ-ϕ bins, nine direct trigger inputs are sent from the electromagnetic calorimeter to the central trigger logic.

The total energy sum of the barrel and of each endcap is formed. The electrical noise of these total energy sums corresponds to energy deposits of $\sim$1.0 GeV. Each signal is discriminated at two thresholds, and the resulting outputs sent to direct trigger inputs. The high thresholds are set at 7 GeV in the barrel and 6 GeV in each endcap, while all three low thresholds are set at 4 GeV.

The logical OR of the barrel and endcap θ-ϕ signals, discriminated at high thresholds, are also sent to direct trigger inputs and are used as stand-alone triggers. The threshold of these θ-ϕ ORs can be substantially lower than those of the total energy sums, because of the small number of analogue channels being summed. The thresholds are 2.6 GeV for θ bins θ_2–θ_5, and 3.0 GeV in the endcaps. These lower energy threshold stand-alone triggers provide a high efficiency for single photon events and for many other final states of e^+e^- collisions.

The threshold for the 144 lower threshold θ-ϕ signals is set at 1.0 GeV. This is to be compared with $\sim$0.5 GeV equivalent electromagnetic energy deposited by a minimum ionising particle (*e.g.* μ) traversing the calorimeter. The rate of the θ-ϕ signals is dominated by noise in the electromagnetic trigger system; it corresponds to an energy deposition of $\sim$0.2 GeV. The spatial coincidences of these θ-ϕ signals with those of the track or time-of-flight trigger systems provide a high trigger efficiency for single particles which shower in the electromagnetic calorimeter.

Fig. 7 shows the typical threshold efficiency curves for the total energy and θ-ϕ sums of the barrel and endcaps. The low and high total energy sums are essentially 100% efficient at 7 and 10 GeV, respectively. The ORs of the barrel and endcap high threshold θ-ϕ signals are fully efficient at 3.5 and 5 GeV, respectively.

2.4 Hadron Calorimeter Trigger

The hadron calorimeter measures the energy of hadrons emerging from the electromagnetic calorimeter and assists in the identification of muons. It is made of welded iron plates, with gaps instrumented with streamer tubes, and provides 4 or more interaction lengths of absorber. The barrel consists of nine layers of limited streamer tube chambers, alternating with eight iron slabs, and spans radii from 3.39 m to 4.39 m. Parts of the yoke support structure are not instrumented, representing 12% of the barrel region ($|\cos\theta| < 0.81$). The hadron calorimeter is closed at each end by a doughnut-shaped endcap, subtending the range $0.81 < |\cos\theta| < 0.91$, where eight layers of chambers alternate with seven slabs of iron. The magnet pole-tips are instrumented with thin multiwire chambers and complete the coverage of the solid angle for hadronic shower detection up to $|\cos\theta| = 0.99$. In order to improve the energy resolution in the forward direction the number of samplings is increased to ten.

In the streamer tube layers, signals are induced onto 4 mm wide aluminium strips as well as onto large area (typically 500 mm × 500 mm) pads. Layers of pads are grouped together to form towers, dividing the solid angle into 48 bins of 7.5° in ϕ and 21 bins in θ. Signals from the layers in each tower are summed by unit gain amplifiers mounted near the chambers, then transmitted to 32-channel ADCs [14], where the charge is integrated for 2.5 μs after beam crossing has occurred. The tower readout ADCs generate analogue sums of 3×4 or 4×4 towers. In the pole-tips, the geometry is more complex, but for trigger purposes, the tower signals are summed to form single θ bins which span 45° in ϕ.

In total, there are 92 analogue sum signals which are arranged in nine circular rings, one with eight ϕ bins covers each pole-tip and each endcap, the remaining five with 12 ϕ bins each cover the barrel. These signals are discriminated at three different thresholds by 18 six-channel comparator cards, each of which serves a half-ring of the detector cylinder. Elements with energies above the lowest threshold are digitally mapped onto the 6×24 overlapping bins of the hadron layer of the θ-ϕ matrix by matching cards, where typically three ϕ bins are set by each hadron trigger element. Signals above the other two thresholds are combined by PAL-based logic cards to generate coincidence signals between the 18 different half-ring sections and will be used as direct trigger inputs.

Since the hadron calorimeter trigger hardware was installed late in the 1990 LEP physics run, it has so far been operated only passively, for debugging and to study applications. Only the barrel part (θ regions θ_2–θ_5) was operational. The results show that the lowest threshold can be comfortably set to 800 MeV, which corresponds to the average energy deposit of a muon traversing just three layers of the calorimeter. At this threshold the total rate was about 200 Hz, largely from natural radioactivity in the calorimeter material and from genuine cosmic ray events. The efficiency for detecting single muons (from $e^+e^- \to \mu^+\mu^-$) within the instrumented region was about 85%.

The direct triggers are still under study, but it appears possible to reduce cosmic rays to a tolerable level with a single-element threshold of ~5 GeV and a coincidence requirement between half-rings on opposite sides of the detector.

2.5 Muon Detector Trigger

Charged particles which have traversed the hadron calorimeter are measured by four layers of muon chambers, split into barrel and endcap parts, which aid in muon identification and contribute to the muon trigger. The barrel and endcap muon detectors together cover about 95% of 4π.

The muon barrel detector consists of 110 large area drift chambers [16] arranged in layers surrounding the magnet return yoke. The coverage of the muon barrel detector is $|\cos\theta| < 0.68$ for

four layers and $|\cos\theta| < 0.72$ for at least one layer. Each chamber has an active volume 1.2 m wide, 15 mm deep, and up to 10.4 m long. It consists of two cells, side by side, each containing an anode wire running the whole length of the chamber and supported every 1.4 m. Electrons drift a maximum distance of 297 mm from either side.

The endcap muon detector [17] covers the angular ranges $\sim 0.67 < |\cos\theta| < \sim 0.985$ and is perpendicular to the beam axis. Each endcap consists of two chambers mounted at a distance apart of about 650 mm. Each chamber consists of two layers of limited streamer tubes, separated by 19 mm, one layer having vertical wires and the other horizontal wires. The streamers produced by traversing charged particles are detected by the charge induced on planes of aluminium strips on both sides of the tubes, thus measuring the x and y coordinates.

The muon detector provides a total of 120 θ-ϕ signals and four direct signals. Since the muon barrel detector has no z measurement for the trigger, the 24 ϕ signals which it provides are used in the θ-ϕ matrix to set simultaneously the four barrel θ bins θ_2 to θ_5. The endcap muon detector provides 96 θ-ϕ signals contributing 24 ϕ signals to each of the theta bins θ_1, θ_2, θ_5 and θ_6. There is only a small amount of overlapping defined in ϕ for the muon detector. This does not cause any loss of θ-ϕ correlations, because full overlapping is used in other subdetectors. The muon barrel detector provides one direct signal which is simply the logical OR of the 24 muon barrel ϕ signals. Two direct signals from the endcap muon detectors are the logical ORs of the 48 θ-ϕ signals from each of the left and right muon endcaps. A third direct signal demands a hit in both endcaps with a loose collinearity requirement, *i.e.* a signal in one end has to be matched by an approximately back-to-back signal in the equivalent θ bin at the other end and at the opposite x coordinate.

Electronics of the Muon Barrel Detector

The front-end electronics of the muon barrel detector provides 220 discriminated signals, one per cell. The 220 signals go to four custom "layer" boards, one board for each layer of barrel chambers. The output of each layer board is 24 ϕ sector signals obtained from ORing up to four cell signals. The chambers on the edge of the definition of a ϕ sector are included in the OR of the adjacent one providing some overlap between them.

The chamber signals terminate in gateable transceivers on the layer boards. The gating of these transceivers is derived from the bunch crossing and is ~ 8 μs long corresponding to the maximum drift time of the chambers. Two Logic Cell Array (LCA) chips per layer board sit on a 56-line bus fed by the transceivers. The two LCAs are programmed to perform 24 latched ORs, one per ϕ sector. The assignment of individual chamber signals to a particular ϕ sector(s) is specified, along with the definition of the 12 latched ORs per chip, in a PROM whose contents are downloaded to the LCA. The LCA latches are cleared just before each bunch crossing. On-board jumpers permit individual chamber signals to be disabled, if desired, and left in a permanent high or low state.

The 4×24 layer ϕ signals are reordered in two "mixer" boards and presented to six VME coincidence modules. Here a 3 out of 4 coincidence is performed on the 4 latched layer ϕ signals for each of the 24 ϕ sectors. These modules also permit individual ϕ sectors to be set for 2/4 or 4/4 coincidences. This option, along with the flexibility designed into the layer boards, permits the optimisation of the trigger efficiency, the ϕ sector overlap, and the noise rate according to the requirements of the experiment.

Performance of the Muon Barrel Trigger

The quiescent rate of the OR of the θ-ϕ signals is about 80 Hz, which is largely due to real cosmic rays with a contribution from inherent chamber noise. A particular cell can be removed from the muon barrel trigger if desired by setting it to a permanent "ON" state, the 3/4 coincidence then effectively being a 2/3 coincidence. The inherent contribution of chamber noise then rises by about 50 Hz per affected ϕ sector. Due to this high rate the muon barrel trigger is used in coincidence only. Its efficiency has been measured to be 95% per muon track within its solid angle acceptance.

Electronics of the Muon Endcap Detector

The charges induced on the aluminium strips by streamers in the active part of the detector are read out at one end of each strip, and they are integrated over 5 μs after beam crossing, this long period giving an acceptable signal to cross-talk ratio. The trigger signals are formed by summing the charge over regions of 64, 96 or 128 adjacent strips in both the x and y directions. The results are compared with a preset threshold to decide if significant activity occurred in the region of the summed channels. Discriminators generate 480 raw trigger signals which are processed further.

An overview of the different stages of signal processing is shown in fig. 8. Track elements are searched along 120 predefined x and y roads, loosely pointing to the vertex. The tracks are graded (using PALs) into four categories: strong, medium, weak and no track; these correspond to 4, 3, 2 or fewer hits along a road, respectively. Where there are only two hits, one must be in each chamber plane separated by the 650 mm lever arm. The resulting 120 signals are then processed via look-up tables to identify active trigger regions. The look-up tables also perform the conversion from the detectors cartesian geometry (x,y) into the polar geometry of the θ-ϕ matrix, introducing some degree of overlapping between the resulting θ-ϕ bins. At this stage, a minimum track grade can be demanded. The final θ-ϕ signals are passed to the central trigger logic 12 μs after the beam crossing.

Performance of the Muon Endcap Trigger

The flexibility in setting the level of coincidence between hits before a final trigger signal is formed, along with an easily adjustable threshold, means that the performance can be tuned to give a high efficiency with good noise rejection. For most of the run, the requirement was just that there be a hit in both x and y in two chambers separated by the 650 mm gap, and that the hits be consistent with a track coming from the interaction region.

The threshold for a trigger signal was set to 1.5 pC, about 3σ above noise arising from the summation over 128 strips, with a noise level of $\sim$0.04 pC from each strip. This is in comparison with an average streamer signal which produces a total charge of $\sim$10 pC.

The efficiency of one streamer tube layer to form a streamer was measured to be $95 \pm 2\%$, as expected from the chamber geometry. The efficiency of the trigger to see the signal of the streamer is $94 \pm 2\%$, giving an efficiency of one raw trigger signal of $89 \pm 3\%$. Since each track can produce four raw trigger signals in each projection of the endcap and only two out of these four are needed in order to make a trigger, the redundancy is high, which implies an overall efficiency of approximately 97% for one track.

The muon endcap trigger rate is dominated by cosmic ray muons; the noise rate in comparison is negligible. In the 1990 run, the rate for either endcap was approximately 20 Hz from cosmic muons satisfying crude pointing to the vertex. The corresponding rate requiring both endcaps in coincidence was approximately 0.2 Hz. This low rate allowed it to be used as a stand-alone muon pair trigger for the endcap region.

2.6 Forward Detector Trigger

The luminosity of the colliding beams is determined by the observation of small angle Bhabha scattering with the forward detectors which surround the beam pipe at either end of the central tracking system. Their acceptance covers angles from 40 to 150 mrad from the beam and 2π in azimuth. The main component of each detector is an electromagnetic calorimeter with a presampler, which provide the essential forward detector trigger signals.

The calorimeter has 35 layers of lead-scintillator sandwich (24 X_o), read out with wavelength shifters, vacuum phototetrodes, charge sensitive preamplifiers and charge integrating ADCs [14]. The front 4 X_o, the presampler, has wavelength shifters at the outside only, but the main calorimeter is read out on both the inner and outer edges. There are sixteen azimuthal segments, giving 48 readout channels per end.

All forward detector triggers demand signals from the calorimeter and therefore rely on the response from a single detector. In order to maintain a certain degree of redundancy the trigger signals are obtained in two different ways.

The first class of trigger signals is derived by discriminating the integrated sum of all 16 segments in each of the calorimeters. The charge integrating ADCs provide analogue outputs which are proportional to the total energy deposited in the main and presampler sections separately. The response of each individual channel in the sum was maintained uniform to within 5% by tuning the high voltage of the phototetrodes. For most of the data taking period the presampler and main signals were summed before discrimination. The energy sum discriminators each have two levels, set to 15 GeV and 35 GeV. The coincidence of the low threshold signals was used as the basic luminosity trigger. A direct trigger input derived from signals exceeding the high threshold in either of the calorimeters was added during the 1990 running period in order to increase the precision with which the efficiency of the coincidence triggers could be determined. The low threshold signals from each side of the detector are also provided separately to the central trigger logic where at least one is required in coincidence with signals from other detectors to provide a trigger for tagged two-photon interactions.

The second class of signals use the main calorimeter analogue signals before they are attenuated and used as inputs to the ADCs. At this point the signals have a rise-time of $\sim$1 μs and a fall-time of $\sim$5 μs, their peak voltage being proportional to energy (12 mV/GeV). Signals from adjacent segments are summed in order to capture at least 95% of the total energy deposited in the main calorimeter by an incident electron, even if it falls directly on a segment boundary. The resulting 16 segment-pair signals in each calorimeter are then discriminated with a threshold of 12 GeV, and the coincidence of any of the directly back-to-back calorimeter segment signals is formed. Since the segment signals are the sum of adjacent segment pairs, the back-to-back condition has a tolerance of about $\pm 45^\circ$ in azimuth.

In addition to these "real" coincidence triggers the forward detector electronics also forms "accidental" triggers using signals delayed with respect to each other by four bunch crossings. The interval of four bunch crossings is chosen so that the accidentals are measured using the same bunch combinations as those which actually collide at the interaction region. The segment and sum accidental coincidences are formed analogously to the real trigger signals. The side which is delayed in the accidental trigger comparison is alternated on each bunch crossing. Thus, a sample of accidental half-events is obtained, where only the latched trigger bits are available from the delayed side of the detector, while the signals from the non-delayed side are digitised as normal. These triggers can be used to estimate the contribution of in-time accidental events in the final luminosity sample.

Due to the clear signature of Bhabha events in the detector and the cleanliness of the LEP beams the forward detector trigger proved to be both efficient and pure. In typical LEP operation with average

total currents of $\sim$1 mA $\times$ $\sim$1 mA and a luminosity of 0.4×10^{31} cm^{-2}s^{-1}, the total rate of luminosity triggers was about 0.5 Hz. Of this rate, 0.2 Hz were valid luminosity events. The accidental rate, monitored by the out-of-time accidental triggers, was typically <0.01 Hz. The low threshold trigger and the segment based triggers imposed a clean energy cut, the hardware threshold resolution being about $\pm$0.5 GeV including the effect of segment-to-segment gain variations and the radial dependence of the raw calorimeter energy response. Using the high threshold signals from either calorimeter, the inefficiency of the trigger for the final fiducial sample of luminosity events, which includes radiative Bhabhas with electron energies as low as 17 GeV, was shown to be negligible (0.05%).

3 The Central Trigger Logic

The central trigger logic is programmable and allows a variety of logical conditions to be imposed on the subdetector signals. All subdetector direct and θ-ϕ input signals are available at the central trigger logic between 1 μs and 14 μs after the bunch crossing. Internal signals are derived from the θ-ϕ signals, which are then combined with the direct signals, and 7 μs before the next bunch crossing a decision is taken whether to accept the associated event. If an event is to be accepted, a trigger signal is sent to the subdetectors which starts their front-end readout. No new triggers are generated until all subdetectors have finished their readout, giving rise to a certain deadtime.

The central trigger logic comprises the following purpose-built VME modules:

- The "Single Input Module" (SIM), which receives the direct signals from the subdetectors.
- Five cards making up the θ-ϕ matrix, one card per subdetector layer.
- The "Pattern Match Module" (PAM), which combines the SIM signals and the θ-ϕ matrix outputs to produce the final trigger decision.
- The "General Trigger Unit" (GTU), which supervises the timing of the subdetectors. "Local Trigger Units" (LTUs) in each subdetector readout crate are connected to the GTU via the trigger bus. They receive the GTU synchronisation and trigger signals and provide the VME interrupt to the subdetector readout systems.
- Additional modules for monitoring input rates, detector status signals and the subdetector readout dead-times.

In addition to beam-synchronised operation, the trigger system allows cosmic ray data to be taken using a gating signal derived from scintillation counters above the detector. Test runs with randomly generated triggers are particularly useful when debugging or setting up.

In the following subsections the modules of the central trigger logic are described in more detail, together with its control, monitoring and performance.

Trigger Crate

The VME cards of the trigger data acquisition system and the purpose-built trigger cards are installed in a dedicated crate, which contains a special internal trigger bus consisting of $\sim$250 extra lines in addition to a standard VME/VSB bus. Up to nine normal-height VME cards and ten purpose-built, double-height trigger modules can be installed. The normal-height VME modules installed in the trigger crate are identical to the ones used in most of the subdetector data acquisition systems; they are a single board computer based on a 68020 microprocessor, a 4 Mbyte dynamic memory, an Ethernet card, and a VME interconnect port [2].

Single Input Module

The single input module (SIM) receives up to 64 direct inputs from the subdetectors as standard NIM signals. It receives a $\sim$15 μs wide gate from the GTU following a bunch crossing, and any of its input signals arriving during this gate are latched and available on the internal trigger bus. They are also stored in registers accessible to the microprocessor in the trigger crate. VME readable 32-bit scalers on a separate module connected to the SIM allow the rates of all SIM inputs to be measured, independently of whether event readout is in progress or not.

θ-ϕ Matrix

Five modules, one for each detector layer which sends signals to the θ-ϕ matrix, receive up to 144 differential signals each on twisted pair flat cables. The inputs can be disabled in groups of eight to remove noisy channels. Programmable Array Logic (PAL) chips are used to form the output signals (see table 4 and fig. 2), which fall into one of the following four classes:

- At least one θ-ϕ bin is above threshold in either endcap (except for the time-of-flight detector) or in the barrel region.
- Multiplicity counting, *i.e.* $\geq$1 and $\geq$2 θ-ϕ bins above threshold, is performed after projection on θ. To avoid double counting due to the overlap of θ-ϕ bins, two adjacent bins are counted as one.
- Hits in back-to-back θ-ϕ bins are recognised for the track trigger, the time-of-flight system, the electromagnetic calorimeter, and the hadron calorimeter.
- Coincidences in depth are formed, *i.e.* coincidences in the same θ-ϕ bins of any two of the five detector layers, except for coincidences between the hadron and electromagnetic calorimeters.

These 35 output signals of the θ-ϕ matrix are available on the internal trigger bus and can also be used as SIM input signals.

Pattern Match Module

The pattern match module (PAM) combines the up to 64 SIM signals and up to 56 θ-ϕ matrix outputs and forms the final trigger decision. At the level of the PAM, these 120 inputs on the internal trigger bus are equivalent and make up the "trigger word", which is sent, for accepted events, to every local trigger unit by the general trigger unit. The PAM employs PALs and look-up memories (RAMs) arranged in several "layers" with identical hardware, but having different PAL settings and RAM contents. Each layer realises a different set of logical conditions, the final trigger decision being the OR of all of them.

Since the layers all work the same way, only one layer of the PAM logic needs to be described. Eight groups of 15 input signals to the PAM logic serve as addresses for eight respective memory look-up tables with 32 kbit each, as indicated in fig. 9. Thus, any arbitrary boolean combination $F_g(\ I_{g,1},\ \ldots\ ,I_{g,15}\ )$ of the 15 inputs of a group, g ($g = 1-8$), can be required by setting the memory contents accordingly. Conditions on the eight respective output signals of the look-up memories are imposed using PALs, *i.e.* a function $T(\ F_1\ ,\ \ldots\ ,F_8\ )$ is performed by the PALs. Restrictions arise from the grouping of input signals; for example, a logical OR of a coincidence of two signals from different groups and a single signal (*e.g.* ($I_{1,15}$ AND $I_{2,15}$) OR $I_{2,14}$), is not possible in one layer.

One card of n layers with n$\times$32 kbytes of look-up memory allows one to have the logical OR of n functions T_1 ... T_n. The version of the PAM used so far had eight layers. Restrictions were minimised by judicious choice of the grouping of input signals and duplication of some θ-ϕ signals. A version with 16 layers and the PALs replaced by look-up memories is in preparation.

Subdetector Synchronisation

The synchronisation of the subdetectors with the central trigger logic is performed by the general trigger unit (GTU) in the trigger crate and Local Trigger Units (LTUs) in each subdetector readout crate. These are connected via the trigger bus, divided into four branches of flat twisted-pair cables.

The GTU controls the timing of the trigger system by providing the strobes necessary to latch the input signals from the various subdetectors as well as internal timing signals for the central trigger logic. The timing is relative to the time of the crossing of the electron and positron bunches inside the detector. A corresponding signal is provided by the LEP machine and is used as the primary gate for the GTU. This gate can be replaced under software control by gating signals derived from a gate generator or a cosmic ray hodoscope, and is distributed to all subdetector LTUs, which are thus synchronised with the central trigger logic.

The GTU receives either a reset or an event interrupt signal from the PAM module $\sim$15 μs after each primary gate. The GTU then broadcasts either a trigger interrupt or a reset signal to the LTUs. Upon reset, the subdetectors clear their front-end modules to accept the next gate. The reset time needed by the slowest subdetector is $\sim$7 μs.

On receipt of a trigger, the subdetectors start the digitisation of the event data, while the LTUs generate VME interrupts and assert the "busy" line on the trigger bus. The 120-bit trigger word and an event number, centrally generated by the GTU, are sent to each LTU via the trigger bus. The LTUs keep their own local event count, which is compared with the global event number. An error condition is generated by the LTU driver software if a mismatch is detected, thus excluding synchronisation errors when parts of the event from different subdetectors are merged at a later stage of the data acquisition chain. The trigger word serves as a first classification of the event and may be used to control readout and monitoring processes performed by the microprocessors in the subdetector crates. Having read the event data into local buffers, the subdetector microprocessors release the LTU busy lines, the wired OR of which prevents the GTU from accepting new triggers. The time during which the trigger system is inactive due to this is measured by a timer on the GTU. If a dead time limit of $\sim$4 s is exceeded, or one of the LTUs fails to acknowledge the trigger interrupt, a VME interrupt to the trigger microprocessor is generated. The individual deadtimes caused by the 28 LTUs in the system are measured by a special timer module in the trigger crate.

The GTU also acts as the local trigger unit of the trigger crate, *i.e.* it generates VME event interrupts and waits for the trigger microprocessor to release the busy signal when all modules of the central trigger logic have been read out.

Each LTU can also be used to control a readout crate independently of the GTU. Running in this "local" mode, the LTU takes gate and trigger pulses from connectors at its front panel (the selection of different gates being software controlled). Local running mode is useful for calibration, debugging and setting-up of subdetectors.

Control and Monitoring

Being part of OPAL's data acquisition system, the trigger crate is connected to the VME tree structured readout system, and, via the Ethernet Local Area Network, to the overall run control, which supplies the relevant run and trigger parameters defined by the operator. Messages are injected into the overall error message handler and enable the operator to take action in case of serious problems. The rates of trigger inputs, θ-ϕ matrix outputs and the PAM decisions as well as their history over a run are available as histograms. This information is valuable to the operator for instantaneous feedback on detector performance and background conditions.

Histograms can be viewed remotely from any workstation in the experiment. In addition, a Macintosh II computer allows access to the trigger crate via a terminal port and also has access to the trigger histograms via a fast memory-map VME link.

Before data taking, all components are checked by writing test patterns to the input registers of all modules and verifying the results in the output registers. After successful completion of these tests the contents of the look-up memories are generated. The necessary information is taken from

a data file containing the assignment of trigger signals to SIM inputs, a description of the PAL logic implemented in the PAM, and the logical conditions to be imposed on the PAM inputs. For every event resulting in a trigger, all SIM and θ-ϕ input signals, the θ-ϕ output signals and the outputs of the PAM layers are read out and stored on mass media together with the event information from all subdetectors. The transfer of trigger signals from the subdetectors to the central trigger logic and the performance of the central trigger logic are therefore easily verified by monitor programs running either online or offline.

A simulation of the central trigger logic is performed online by the trigger microprocessor on all triggered events. By repeating the hardware decisions of the trigger modules in software, errors are detected immediately and action can be taken by the operator.

The trigger definition, run parameters and possible errors inside the central trigger logic are stored in a database and are available when events are reconstructed offline. The most important histograms and a breakdown of the contribution of individual signals and coincidences to the overall trigger rate, integrated over a full run, are stored in various databases and facilitate monitoring of the run conditions.

4 Performance of the Trigger System

The trigger rate is a function of the machine luminosity and of beam-related backgrounds; cosmic rays and detector noise contribute a constant fraction, relatively less important as machine currents and luminosity increase. The trigger conditions of the experiment were optimised to provide good efficiency for all considered physics processes and to keep the trigger rate below the maximum rate tolerable by the data acquisition system. During the first months of operation in 1989, new components were included as they became available. The stable running of LEP and low backgrounds allowed a rather stable set of trigger conditions to be used during most of the 1990 running, thereby also facilitating the analysis of the data.

The typical 1990 trigger conditions are shown in table 5 – the rates of the input signals to the final decision logic are given in tables 3 and 4. Redundancy for all physics processes was achieved by triggers based on one detector component only and by triggers sensitive to single particles. This allowed direct measurements of the efficiencies of the various components and led to a high overall performance. Direct signals and back-to-back θ-ϕ signals from the track trigger, the electromagnetic calorimeter, the endcap muon chambers and, particularly in the early running, the time-of-flight detector provided independent triggers with high component efficiencies for pairs of particles or multihadronic events. Efficient single particle triggers and the lowest possible thresholds in the calorimeters were achieved by triggering on spatial correlations between hits in different detector layers; this also provided good sensitivity to rare or new phenomena. The efficiency in the endcap region was increased by triggering on a muon hit or electromagnetic energy on one end of the detector and a track on the opposite end or in the barrel region.

Single particle triggers from only one detector were not possible due to high rates, except for the single cluster trigger in the electromagnetic calorimeters with a threshold of 2.6 GeV and 3.0 GeV in the barrel and endcaps, respectively. The rates of the low threshold electromagnetic triggers and the muon barrel trigger were mainly due to noise, while the track trigger and the time-of-flight system were dominated by beam related backgrounds, and the muon endcap detector was largely dominated by cosmic rays. The rates of all direct signals, θ-ϕ matrix outputs and of the active coincidences are given in tables 3, 4 and 5, averaged over a typical 1990 LEP fill. It is seen that signals requiring only one hit in a detector layer were running at relatively high rates. The θ-ϕ coincidences between detector

layers, however, had low rates, even for low calorimeter thresholds, because the coincidences suppressed random noise or low energy background seen in only one detector layer. The vertex constraint imposed by the track trigger or the narrow time window during which the time-of-flight detector was sensitive rejected cosmic rays in the track/muon and the time-of-flight/muon coincidences, respectively.

The trigger efficiency for $e^+e^- \rightarrow \mu^+\mu^-$ events in the acceptance region $|\cos\theta| < 0.95$ was found to be $99.9 \pm 0.1\%$ [18]. In the endcap region, any two of the expected four trigger signals per $\mu^+\mu^-$ event, from the left and right muon chambers and tracks in the left and right hemispheres, were sufficient to accept an event. In the barrel, events were accepted if they had two tracks, or at least two hits in the same bin of the θ-ϕ matrix in the track trigger, the time-of-flight detector or the muon detector. The efficiencies of the components was determined from events triggered independently by the other components, and the overall efficiency was determined by combining the component efficiencies in bins of $\cos\theta$ or ϕ. The number of $e^+e^- \rightarrow \mu^+\mu^-$ events which were triggered by only one of the above conditions was found to be consistent with the efficiency given above.

Similar considerations hold for the channel $e^+e^- \rightarrow e^+e^-$, where the rôle of the muon detector is taken by the electromagnetic calorimeter. The high efficiency of the electromagnetic calorimeter and of the additional stand-alone electromagnetic triggers led to an overall efficiency of 100%. In the $e^+e^- \rightarrow \tau^+\tau^-$ channel, the total energy of the particles is lower than the centre-of-mass energy of the beams due to undetected neutrinos. The efficiency was found to be $99.9 \pm 0.1\%$ for events with a "visible energy" (the scalar sum of the energy in the electromagnetic calorimeter and the track momenta measured by the central detector) greater than 18% of the centre-of-mass energy. The efficiency for multihadronic events was >99.9% within the 98% acceptance of the offline analysis [18]. A collection of trigger efficiencies for the main physics channels can be found in table 6.

The main trigger on Z^0 decays into two neutrinos with one radiative initial state photon was provided by the spatial coincidence of the time-of-flight detector and the electromagnetic calorimeter, with a threshold of 1 GeV for photons which start showering in the material before the time-of-flight detector (about 80% of all photons). At higher photon energies, the single cluster trigger of the electromagnetic barrel calorimeter with a threshold of 2.6 GeV also contributed. A further trigger, sensitive to lower energy photons and requiring a shower in the magnet coil, was obtained by demanding two or more time-of-flight counters within $\sim 60°$ in ϕ (three standard overlapping ϕ bins), no other counters in the opposite $\sim 300°$ and fewer than eight hits in jet chamber ring 1. The threshold behaviour of these triggers was studied using events with a single electron in the barrel region, from the process $e^+e^- \rightarrow e(e)\gamma$, which were also triggered by the track/electromagnetic and the track/time-of-flight θ-ϕ coincidences. In the barrel region, an overall trigger efficiency of $98.7 \pm 0.1\%$ for photons interacting in the magnet coil and with deposited energies above 1.5 GeV was found [20].

Since all searches for new particles involve looking for conventional particles, with some missing energy compared to the full energy of the colliding beams, the expected trigger efficiencies for *e.g.* leptonic or hadronic events containing Higgs particles [21], decays of the Z^0 into supersymmetric particles [22], or new leptons [23], were also found to be very high (>95% within the analysis cuts).

Random triggers at a prescaled rate of the LEP beam crossing signal in coincidence with all possible low thresholds were taken to measure the rates of new or less restrictive triggers before they were actually enabled. A totally unbiased random trigger at a rate of 0.04 Hz provided samples of "empty" events, which were used to monitor noise hits in some subdetectors as well as for online pedestal adjustment.

Trigger Rates

With the above trigger conditions and a typical machine luminosity of 0.4×10^{31} $cm^{-2}s^{-1}$, the average trigger rate was about 2 Hz, decreasing from ~2.5 Hz at the beginning to ~1.5 Hz towards the end of the fill. The rate of multihadronic events was 0.12 Hz (on the Z^0 resonance), and the rate of genuine forward detector Bhabha events was 0.2 Hz. Z^0 decays into pairs of charged leptons contributed another 0.02 Hz. Cosmic rays and triggers originating from noise contributed ~0.6 Hz. The rest of the rate was caused by beam-wall and beam-gas interactions, off-momentum particles, beam halo muons produced at the various collimators, and synchrotron radiation. The dominating contributions to triggers induced by beam background originated from the stand-alone time-of-flight triggers (~20%) and from the forward detector (~15%).

5 Summary

The OPAL trigger system provided a high efficiency from the first collisions in LEP onwards. Lower trigger thresholds and an increased sensitivity and homogeneity were achieved during 1989 and the beginning of the 1990 running period. This allowed the physics analyses of low-multiplicity events to be extended into the endcap regions, with small systematic errors due to trigger inefficiencies, thus well matching the increased statistics delivered by the LEP machine. The high flexibility of the trigger system in combination with good monitoring allowed us to adapt the trigger to maintain both a high efficiency and a tolerable rate, while the boundary conditions such as machine luminosity, backgrounds and detector noise varied.

Acknowledgements

The successful design, construction and commissioning of the trigger system would not have been possible without the tremendous efforts of all our technical collaborators in the participating institutes, and we warmly thank them for their dedication and support over the last years. It is a pleasure to thank the SL Division for the efficient operation of the LEP accelerator and for the clean beam conditions they delivered to the experiment.

We gratefully acknowledge the financial support of the following: The Bundesministerium für Forschung und Technologie, FRG, The Department of Energy, USA, The Direction des Sciences de la Matiere (DSM), France, The Israeli Ministry of Science, The National Science Foundation, USA, The Japanese Ministry of Education, Science and Culture (the Monbusho) and a grant under the Monbusho International Science Research Program, and The Science and Engineering Research Council, UK.

References

[1] OPAL Technical Proposal, CERN/LEPC/83-4.
OPAL Collaboration, K. Ahmet et al., CERN-PPE/90-114,
to be published in Nucl. Instr. and Meth.

[2] "The OPAL Data Acquisition System",
paper in preparation, to be submitted to Nuclear Instruments and Methods A.

[3] IEEE 1014/D1.0.

[4] "An Online Filter and Second-Level Trigger for the OPAL Experiment at LEP",
paper in preparation.

[5] J.M. Roney et al., Nucl. Instr. and Meth. A279 (1989) 236.
J.M. Roney, Ph.D. Thesis, Carleton University, unpublished.

[6] H.M. Fischer et al., Nucl. Instr. and Meth. A252 (1986) 331.
R.-D. Heuer and A. Wagner, Nucl. Instr. and Meth. A265 (1988) 11.
H.M. Fischer et al., Nucl. Instr. and Meth. A283 (1989) 492.

[7] A.A. Carter et al., Nucl. Instr. and Meth. A250 (1986) 503.

[8] A.A. Carter et al., Nucl. Instr. and Meth. A286 (1990) 107.

[9] R. Humpert, Diploma Thesis, Universität Freiburg, unpublished.

[10] B. Hallgren and H. Verweij, IEEE Trans. Nucl. Sci., NS-27 (1980) 333.

[11] M.J. French and F. Slorach, Proceedings of the International Conference on The Impact of Digital Microelectronics and Microprocessors on Particle Physics, Trieste, Italy, (1988) 181.

[12] M. Akrawy et al., Nucl. Instr. and Meth. A290 (1990) 76.
M. Akrawy et al., paper in preparation, to be submitted to Nuclear Instruments and Methods A.

[13] M.D. Rousseau et al., IEEE Trans. Nucl. Sci., NS-30 (1983) 479.

[14] A. Beer, G. Critin and G. Schuler, Nucl. Instr. and Meth. A234 (1985) 294.
F. Bourgeois et al., IEEE Trans. Nucl. Sci., NS-34 (1987) 240.
G. Schuler, "96-Channel FASTBUS Charge Integrating ADC CIAFB F683C",
CERN/EF/4102H/GS/ed (1988).

[15] G. Schuler, "ANAMAT FASTBUS Linear Summing Module",
CERN/EF/ in preparation.

[16] J. Allison et al., paper in preparation, to be submitted to Nuclear Instruments and Methods A.

[17] G.T.J. Arnison et al., Nucl. Instr. and Meth. A294 (1990) 431.

[18] OPAL Collaboration, M.Z. Akrawy et al.,
paper in preparation, to be submitted to Zeitschrift für Physik C.

[19] OPAL Collaboration, M.Z. Akrawy et al., CERN-PPE/90-189 (18 December 1990),
to be published in Phys. Lett. B.

[20] OPAL Collaboration, M.Z. Akrawy et al., CERN-PPE/90-187 (14 December 1990),
to be published in Z. Phys. C.

[21] OPAL Collaboration, M.Z. Akrawy et al., Z. Phys. C49 (1990) 1.
OPAL Collaboration, M.Z. Akrawy et al., Phys. Lett. 251B (1990) 211.

[22] OPAL Collaboration, M.Z. Akrawy et al., Phys. Lett. 240B (1990) 261.
OPAL Collaboration, M.Z. Akrawy et al., Phys. Lett. 242B (1990) 299.
OPAL Collaboration, M.Z. Akrawy et al., Phys. Lett. 248B (1990) 211.

[23] OPAL Collaboration, M.Z. Akrawy et al., Phys. Lett. 240B (1990) 250.
OPAL Collaboration, M.Z. Akrawy et al., Phys. Lett. 242B (1990) 135.
OPAL Collaboration, M.Z. Akrawy et al., Phys. Lett. 247B (1990) 448.

θ bin	cos θ range	ϕ bin	ϕ range
1	-0.980 - -0.596	1	0° - 30°
2	-0.823 - -0.213	2	15° - 45°
3	-0.596 - 0.213	3	30° - 60°
4	-0.213 - 0.596	...	...
5	0.213 - 0.823	23	330° - 360°
6	0.596 - 0.980	24	345° - 15°

Table 1: θ-ϕ Segmentation of the Detector at the Trigger Level
The ϕ segmentation is matched only approximately by some subdetectors, see table 2.

Subdetector	ϕ_0	ϕ width	Number of bins
track trigger	0°	30°	12
	15°	30°	12
time-of-flight	0°	36°	1
and	9°	36°	1
electromagnetic barrel	27°	36°	1
	The above pattern is repeated 7 more times, at 45°, 90°, 135°, 180°, 225°, 270° and 315°.		
electromagnetic endcap	+2°	30°	12
left	+17°	30°	12
electromagnetic endcap	-2°	30°	12
right	+13°	30°	12
hadron barrel	0°	30°	12
hadron endcap and pole tip	0°	45°	8
muon barrel	~-3.5°	~22° *	24
muon endcap	~0°	~25° *	24
	*) bins are partially overlapping		

Table 2: Subdetector Segmentation in ϕ.
The start value of a repetitive pattern of ϕ segments is denoted ϕ_0.

Signal description	Detector	Name	Rate (Hz)
$\geq$ 1 track	TT	TM1	8
$\geq$ 2 tracks	TT	TM2	1
$\geq$ 3 tracks	TT	TM3	0.2
$\geq$ 1 barrel track	TT	TBM1	0.4
$\geq$ 2 barrel tracks	TT	TBM2	0.2
$\geq$ 3 barrel tracks	TT	TBM3	0.1
$\geq$ 8 hits in vertex chamber	TT	VXH	400
$\geq$ 8 hits in jet chamber ring 1	TT	J1H	150
$\geq$ 8 hits in jet chamber ring 2	TT	J2H	70
$\geq$ 8 hits in jet chamber ring 3	TT	J3H	50
track with low charge (free quark)	TT	QUARK	0.01
track with high charge (magnetic monopole)	TT	MONOPOL	0.02
$\geq$ 1 time-of-flight hit	TOF	TOFOR	20
$\geq$ 7 overlapping TOF θ-ϕ bins	TOF	TOFMANY	0.2
number of TOF bars hit above threshold	TOF	TOFMUL	2
total em energy in barrel $\geq$ 7 GeV	EM	EBTOTHI	0.1
em energy in left endcap $\geq$ 6 GeV	EM	EELHI	0.06
em energy in right endcap $\geq$ 6 GeV	EM	EERHI	0.06
em energy in barrel $\geq$ 4 GeV	EM	EBTOTLO	10
em energy in left endcap $\geq$ 4 GeV	EM	EELLO	0.5
em energy in right endcap $\geq$ 4 GeV	EM	EERLO	0.5
$\geq$ 1 θ-ϕ in barrel above 2.6 GeV	EM	EBTPHI	0.2
$\geq$ 1 θ-ϕ in left endcap above 3 GeV	EM	EELTPH	0.1
$\geq$ 1 θ-ϕ in right endcap above 3 GeV	EM	EERTPH	0.1
$\geq$ 1 muon in barrel	MU	MBH	500
$\geq$ 1 muon in left endcap	MU	MEL	20
$\geq$ 1 muon in right endcap	MU	MER	20
$\geq$ 1 muon in left AND right endcaps	MU	MELR	0.2
left AND right energy sum $\geq$ 15 GeV	FD	FDSUM	0.3
left AND right segments $\geq$ 13 GeV	FD	FDSEG	0.35
one forward calorimeter $\geq$ 35 GeV	FD	FDHIOR	0.3
FDSUM accidental trigger	FD	FDSUMA	0.05
FDSEG accidental trigger	FD	FDSEGA	0.005
Energy in left forward calorimeter $\geq$ 15 GeV	FD	LCALLO	4
Energy in right forward calorimeter $\geq$ 15 GeV	FD	RCALLO	4
Prescaled random beam crossing	CTL	BXRSA	0.04
Random beam crossing	CTL	BXR	4

Table 3: Direct Trigger Signals Provided by the Subdetectors
The rates given in column 4 correspond to a typical fill (luminosity of 0.4×10^{31} $cm^{-2}s^{-1}$ and about 1 mA current per beam). The abbreviations in column 2 denote the track trigger (TT), the time-of-flight detector (TOF), the electromagnetic calorimeter (EM) and the muon detector (MU).

Signal description	Name	Rate (Hz)
Track trigger, $\geq$ 1 θ-ϕ in θ_{2-5} (barrel)	TPTTB	1
Track trigger, $\geq$ 1 θ-ϕ bin	TPTT1	8
Track trigger, $\geq$ 2 independent θ-ϕ bins	TPTT2	1
Track trigger, $\geq$ 1 ϕ bin in θ_1	TPTTL	5
Track trigger, $\geq$ 1 ϕ bin in θ_6	TPTTR	5
Track trigger, $\geq$ 1 pair of collinear tracks	TPTTCL	0.15
Track trigger AND TOF, $\geq$ 1 correlated θ-ϕ bin	TPTTTO	0.3
Track trigger AND EM, $\geq$ 1 correlated θ-ϕ bin	TPTTEM	0.15
Track trigger AND Hadron, $\geq$ 1 correlated θ-ϕ bin	TPTTHA	-
Track trigger AND Muon, $\geq$ 1 correlated θ-ϕ bin	TPTTMU	0.03
TOF, $\geq$ 1 θ-ϕ bin	TPTO1	20
TOF, $\geq$ 2 independent θ-ϕ bins	TPTO2	2
TOF, $\geq$ 1 pair of coplanar hits	TPTOCL	0.4
TOF AND EM, $\geq$ 1 correlated θ-ϕ bin	TPTOEM	0.25
TOF AND Hadron, $\geq$ 1 correlated θ-ϕ bin	TPTOHA	-
TOF AND Muon, $\geq$ 1 correlated θ-ϕ bin	TPTOMU	0.2
EM, $\geq$ 1 θ-ϕ bin in barrel	TPEMB	100
EM, $\geq$ 1 θ-ϕ bin	TPEM1	120
EM, $\geq$ 2 independent θ-ϕ bins	TPEM2	0.2
EM,$\geq$ 1 ϕ bin in θ_1	TPEML	10
EM,$\geq$ 1 ϕ bin in θ_6	TPEMR	10
EM, $\geq$ 1 pair of collinear clusters	TPEMCL	0.15
EM AND Muon, $\geq$ 1 correlated θ-ϕ bin	TPEMMU	-
Hadron, $\geq$ 1 θ-ϕ bin in barrel	TPHAB	200
Hadron, $\geq$ 1 θ-ϕ bin	TPHA1	-
Hadron, $\geq$ 2 independent θ-ϕ bins	TPHA2	-
Hadron, $\geq$ 1 ϕ bin in θ_1	TPHAL	-
Hadron, $\geq$ 1 ϕ bin in θ_6	TPHAR	-
Hadron, $\geq$ 1 pair of collinear clusters	TPHACL	-
Hadron AND Muon, $\geq$ 1 correlated θ-ϕ bin	TPHAMU	-
Muon, $\geq$ 1 θ-ϕ bin in barrel	TPMUB	500
Muon, $\geq$ 1 θ-ϕ bin	TPMU1	500
Muon, $\geq$ 2 independent θ-ϕ bins	TPMU2	10
Muon, $\geq$ 1 ϕ bin in θ_1	TPMUL	20
Muon, $\geq$ 1 ϕ bin in θ_6	TPMUR	20

Table 4: θ-ϕ Matrix Output Signals
The rates in column 3 correspond to a typical fill. The signals where no rates are given have not been used in data-taking.

Trigger Condition	Name	Rate (Hz)
More than 3 tracks	TM3	0.2
More than 2 tracks in barrel region	TBM2	0.2
Track trigger collinear θ-ϕ bins	TPTTCL	0.15
Track Trigger - TOF θ-ϕ coincidence	TPTTTO	0.3
Track Trigger - EM θ-ϕ coincidence	TPTTEM	0.15
Track Trigger - Muon θ-ϕ coincidence	TPTTMU	0.03
Track with low charge	QUARK	0.01
Track with high charge	MONOPOL	0.02
$\geq$ 7 overlapping TOF θ-ϕ bins	TOFMANY	0.2
TOF - Muon θ-ϕ coincidence	TPTOMU	0.2
TOF - EM θ-ϕ coincidence	TPTOEM	0.25
TOF-based single photon trigger	TOFMUL.AND. .NOT.(TPTO2.OR.J1H)	0.1
Total energy in barrel region $\geq$ 7 GeV	EBTOTHI	0.1
Total energy in left or right EM endcaps $\geq$ 6 GeV	EELHI.OR.EERHI	0.1
One or more EM θ-ϕ bins in barrel with $\geq$ 2.6 GeV	EBTPHI	0.2
$\geq$ 1 EM θ-ϕ bins in either endcap with $\geq$ 3 GeV	EELTPH.OR.EERTPH	0.15
Electromagnetic calorimeter, collinear θ-ϕ bins	TPEMCL	0.15
$\geq$ 4 GeV in EM endcap AND in barrel	EEL(R)LO.AND.EBTOTLO	0.03
$\geq$ 4 GeV in both EM endcaps	EELLO.AND.EERLO	0.04
$\geq$ 4 GeV in EM endcap AND track on opposite side	EEL(R)LO.AND.TPTTR(L)	0.08
$\geq$ 4 GeV in EM endcap AND $\geq$ 1 barrel track	EEL(R)LO.AND.TBM1	0.05
EM endcap θ-ϕ bin AND $\geq$ 1 barrel track	TPEML(R).AND.TBM1	0.10
EM endcap θ-ϕ AND track on opposite side	TPEML(R).AND.TPTTR(L)	0.15
$\geq$ 4 GeV in EM barrel AND barrel track or TOF hit	EBTOTLO.AND. (TOFOR.OR.TBM1)	0.2
Muon in left AND right muon endcaps	MELR	0.2
$\geq$ 1 endcap muon AND one barrel track or TOF hit	MEL(R).AND. (TBM1.OR.TOFOR)	0.2
Muon in one endcap AND track on the opposite side	MEL(R).AND.TPTTR(L)	0.02
Forward detector energy on both sides above 15 GeV	FDSUM	0.35
Forward detector segments back-to-back, $\geq$ 13 GeV	FDSEG	0.3
Forward detector energy on one side $\geq$ 35 GeV	FDHIOR	(prescaled)
Forward detector accidental	FDSEGA	0.005
$\geq$ 15 GeV in forward cal. AND EM barrel $\geq$ 4 GeV	L(R)CALLO.AND.EBTOTLO	0.04
$\geq$ 15 GeV in forward cal. AND $\geq$ 1 barrel track	L(R)CALLO.AND.TBM1	0.03
Random beam crossing	BXRSA	0.04
Random beam crossing AND any low threshold	BXR.AND. (low thresholds)	$< 4\times0.01$

Table 5: 1990 Trigger Conditions
The rates in column 3 are averages over a typical fill and are not exclusive; the average trigger rate was 2 Hz and decreased from ~2.5 Hz at the beginning of a fill to ~1.5 Hz towards the end.

Physics channel	$\lvert\cos\theta\rvert$	Efficiency (%)
$e^+e^- \rightarrow$ hadrons	<1.0	100
$e^+e^- \rightarrow \mu^+\mu^-$	<.95	99.9 ± 0.1
$e^+e^- \rightarrow \tau^+\tau^-$	<.90	99.9 ± 0.1
$e^+e^- \rightarrow e^+e^-$	<.85	100
$e^+e^- \rightarrow \gamma\gamma$	<.90	>99.9
small angle Bhabha	.989–.999	>99.9

Table 6: Trigger efficiency for different physics channels
The acceptance of the current analysis of each physics channel [18,19] is determined by the solid angles quoted as well as by analysis cuts particular to each channel (mainly important for the multihadronic and $\tau\tau$ channels). The trigger efficiency is for events within this acceptance and is calculated from the data using the inherent redundancy of the trigger system.

Figure Captions

Fig. 1: General Layout of the OPAL Detector

Fig. 2: Overview of Trigger Generation by the θ-ϕ Matrix
The track trigger (TT), the time-of-flight system (TOF), the electromagnetic calorimeter (EM), the hadron calorimeter (HA) and the muon detector (MU) send signals to the θ-ϕ matrix. Crosses on the vertical lines, representing different particle types passing through the detector, indicate the sensitivity at the trigger level.

Fig. 3: Overview of Event Triggering
Discriminated analogue sums or multiplicity counts and θ-ϕ information are provided by the subdetectors after each crossing of the particle bunches. Logical combinations of these, formed in the central trigger logic, lead to a decision whether to accept or reject the associated event. The decision is broadcast by the general trigger unit (GTU) to local trigger units (LTUs) at the subdetectors.

Fig. 4: Principle of Track Finding in the r-z Plane in the Track Trigger Logic
The track trigger electronics forms histograms of the ratio of z and r for four groups of 12 wires in each 15° ϕ sector. For tracks originating from the interaction region the z/r distribution shows a narrow peak, whereas it is flat for other tracks.

Fig. 5: Logic Diagram of z Measurement and Charge Determination Performed by the Trigger Electronics of the Jet Chamber

Fig. 6: Logic Diagram of Histogrammer Modules of the Track Trigger Processor
The z/r values from adjacent sectors, provided by the trigger electronics of the vertex chamber and the jet chamber, are added (ϕ overlap) and smeared over adjacent z/r slices. The track decisions in 30 z/r slices are then combined into six θ bins.

Fig. 7: Efficiency Curves for the Electromagnetic Trigger Signals
The efficiencies for the direct signals provided by the barrel and endcap electromagnetic calorimeters are shown as a function of deposited energy.

Fig. 8: Different Stages of Decision-Making in the Trigger Electronics of the Endcap Muon Detector

Fig. 9: Schematic Layout of the PAttern Match (PAM) Logic
Up to 64 direct signals and up to 56 θ-ϕ signals are arranged in eight groups of 15 inputs each. Look-up memories impose logical conditions on the 15 inputs of each group. The outputs are combined in a second stage by PALs (or another look-up memory in a later version of the module). The same logic is implemented in several layers in order to allow enough flexibility when combining signals connected to different groups. The layer outputs can optionally be prescaled before they are ORed to form the overall trigger decision. Arrows indicate which parts of the logic are accessible via VME.

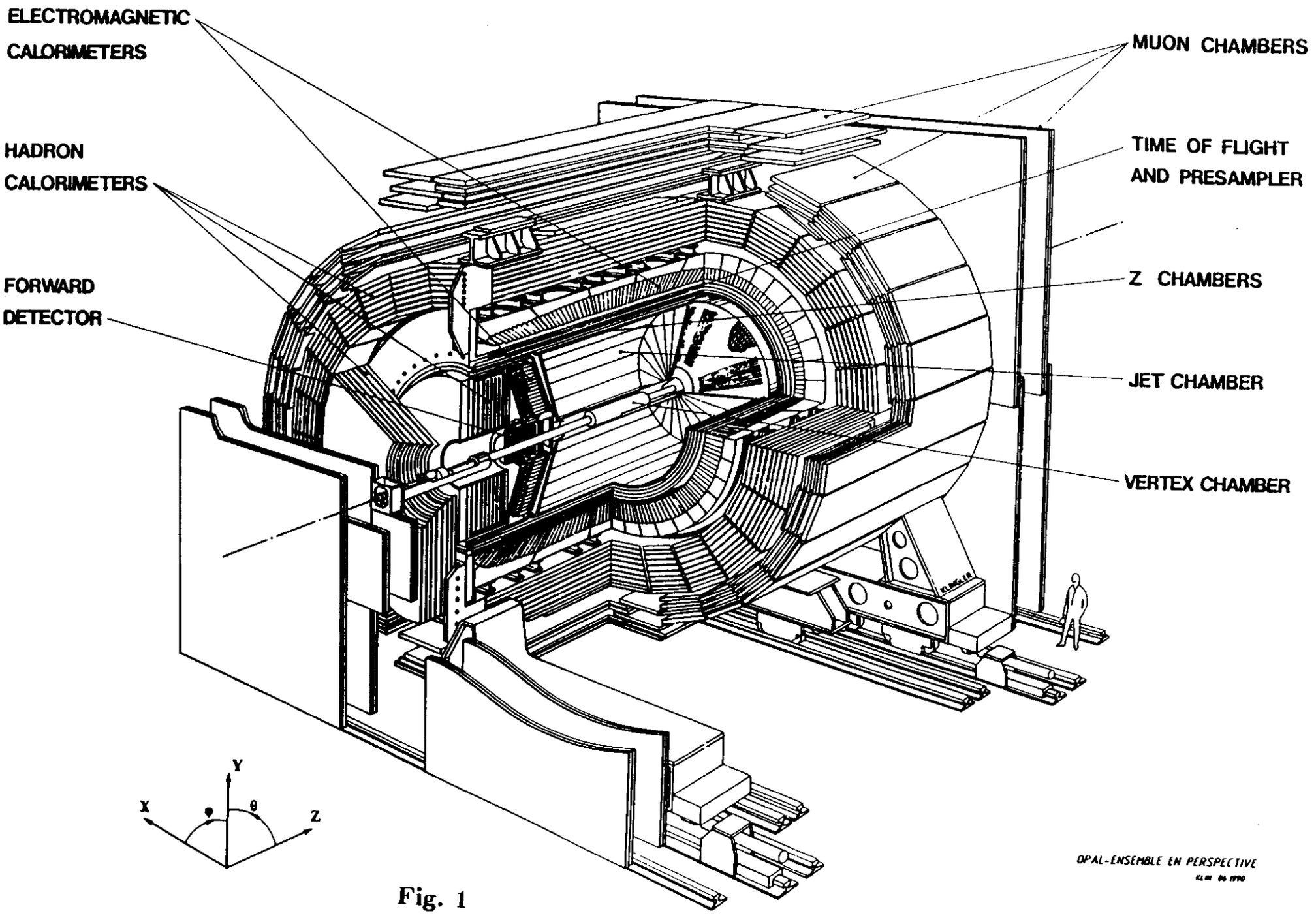
ELECTROMAGNETIC
CALORIMETERS
HADRON
CALORIMETERS
FORWARD
DETECTOR
MUON CHAMBERS
TIME OF FLIGHT
AND PRESAMPLER
Z CHAMBERS
JET CHAMBER
VERTEX CHAMBER
Y
X
Z
θ
OPAL-ENSEMBLE EN PERSPECTIVE

Fig. 1

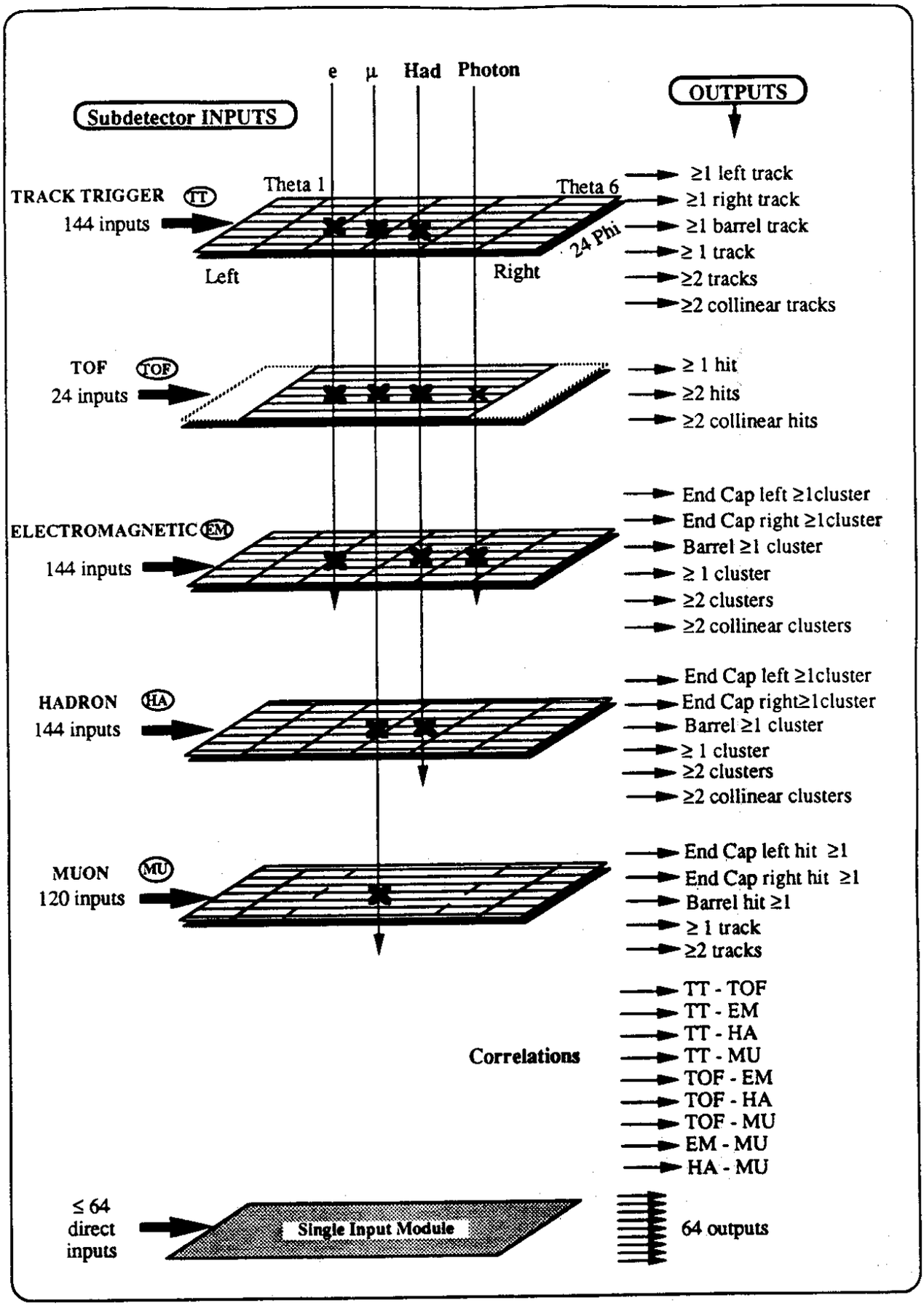
e
μ
Had
Photon
Subdetector INPUTS
OUTPUTS
TRACK TRIGGER TT
144 inputs
Theta 1
Theta 6
24 Phi
Left
Right
≥1 left track
≥1 right track
≥1 barrel track
≥ 1 track
≥2 tracks
≥2 collinear tracks
TOF TOF
24 inputs
≥ 1 hit
≥2 hits
≥2 collinear hits
ELECTROMAGNETIC EM
144 inputs
End Cap left ≥1cluster
End Cap right ≥1cluster
Barrel ≥1 cluster
≥ 1 cluster
≥2 clusters
≥2 collinear clusters
HADRON HA
144 inputs
End Cap left ≥1cluster
End Cap right≥1cluster
Barrel ≥1 cluster
≥ 1 cluster
≥2 clusters
≥2 collinear clusters
MUON MU
120 inputs
End Cap left hit ≥1
End Cap right hit ≥1
Barrel hit ≥1
≥ 1 track
≥2 tracks
Correlations
TT - TOF
TT - EM
TT - HA
TT - MU
TOF - EM
TOF - HA
TOF - MU
EM - MU
HA - MU
≤ 64
direct
inputs
Single Input Module
64 outputs

Fig. 2

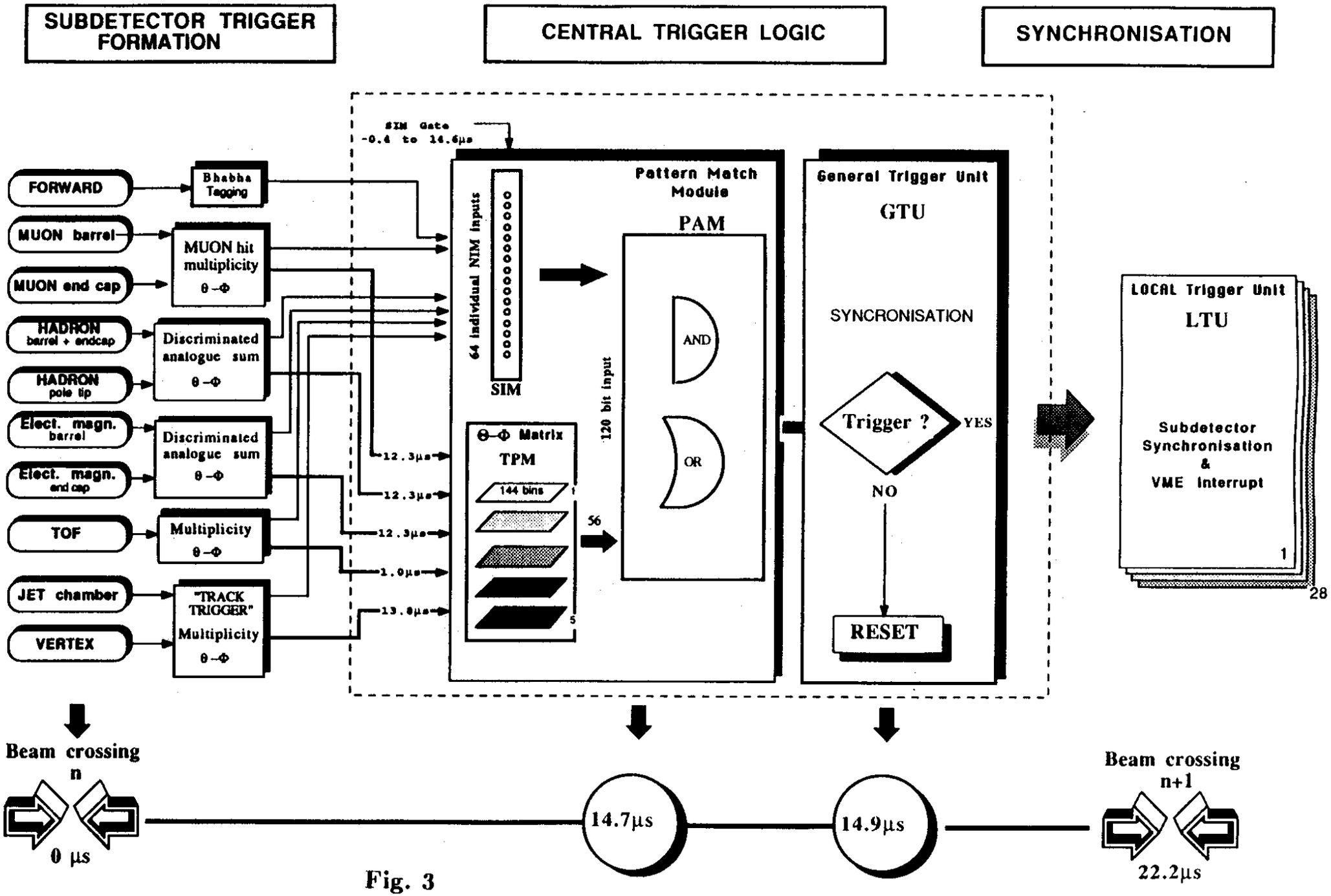
SUBDETECTOR TRIGGER FORMATION
CENTRAL TRIGGER LOGIC
SYNCHRONISATION
SIM Gate
-0.4 to 14.6µs
FORWARD
Bhabha Tagging
MUON barrel
MUON end cap
MUON hit multiplicity θ-Φ
HADRON barrel + endcap
HADRON pole tip
Discriminated analogue sum θ-Φ
Elect. magn. barrel
Elect. magn. end cap
Discriminated analogue sum θ-Φ
TOF
Multiplicity θ-Φ
JET chamber
VERTEX
"TRACK TRIGGER" Multiplicity θ-Φ
64 individual NIM inputs
SIM
Pattern Match Module
PAM
120 bit input
AND
OR
θ-Φ Matrix
TPM
144 bins
56
12.3µs
12.3µs
12.3µs
1.0µs
13.8µs
General Trigger Unit
GTU
SYNCRONISATION
Trigger ?
YES
NO
RESET
LOCAL Trigger Unit
LTU
Subdetector Synchronisation & VME Interrupt
1
28
Beam crossing n
0 µs
14.7µs
14.9µs
Beam crossing n+1
22.2µs

Fig. 3

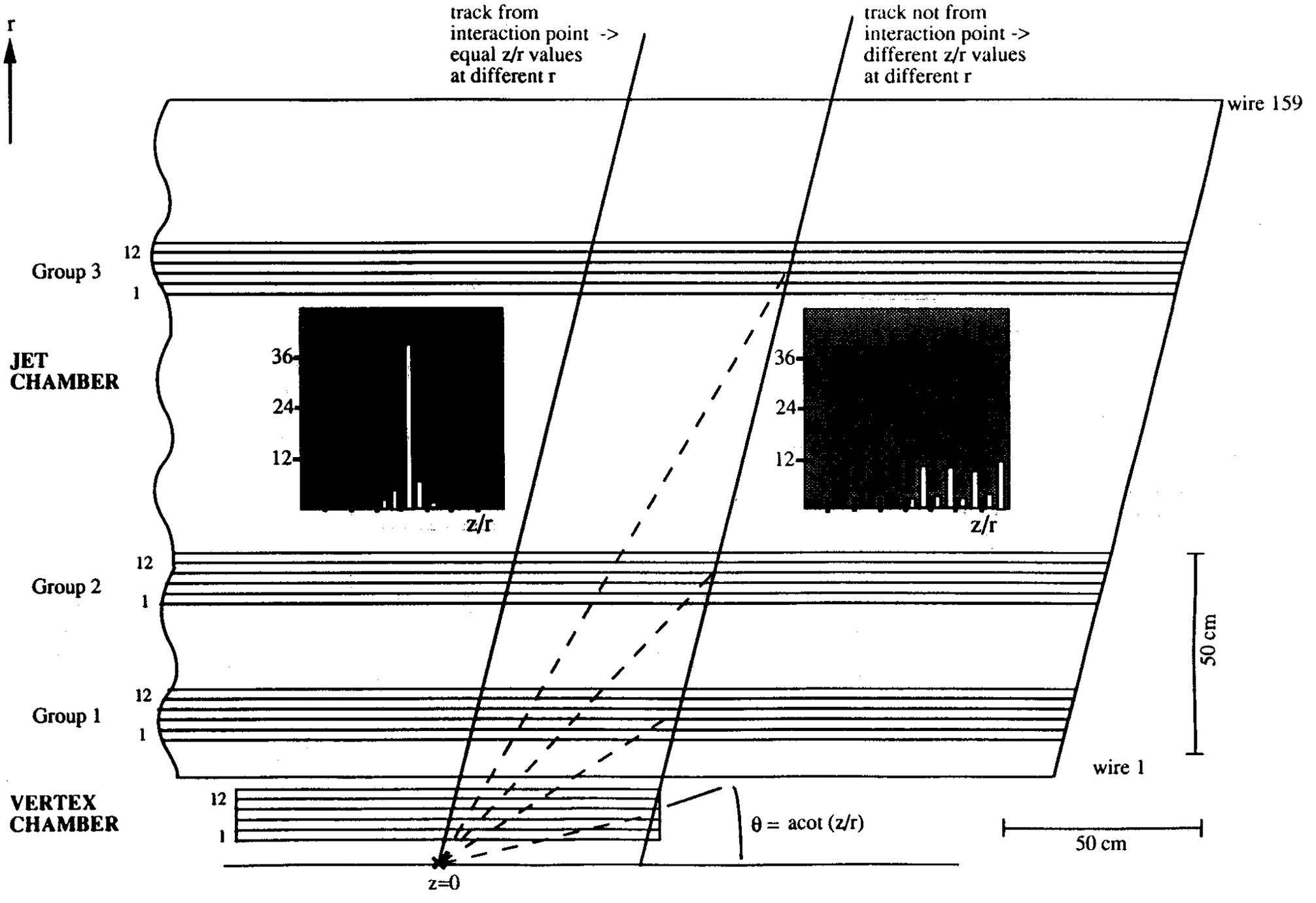
r
track from
interaction point ->
equal z/r values
at different r
track not from
interaction point ->
different z/r values
at different r
wire 159
Group 3
12
1
JET
CHAMBER
36
24
12
z/r
36
24
12
z/r
Group 2
12
1
Group 1
12
1
50 cm
wire 1
VERTEX
CHAMBER
12
1
θ = acot (z/r)
50 cm
z=0
z

Fig. 4

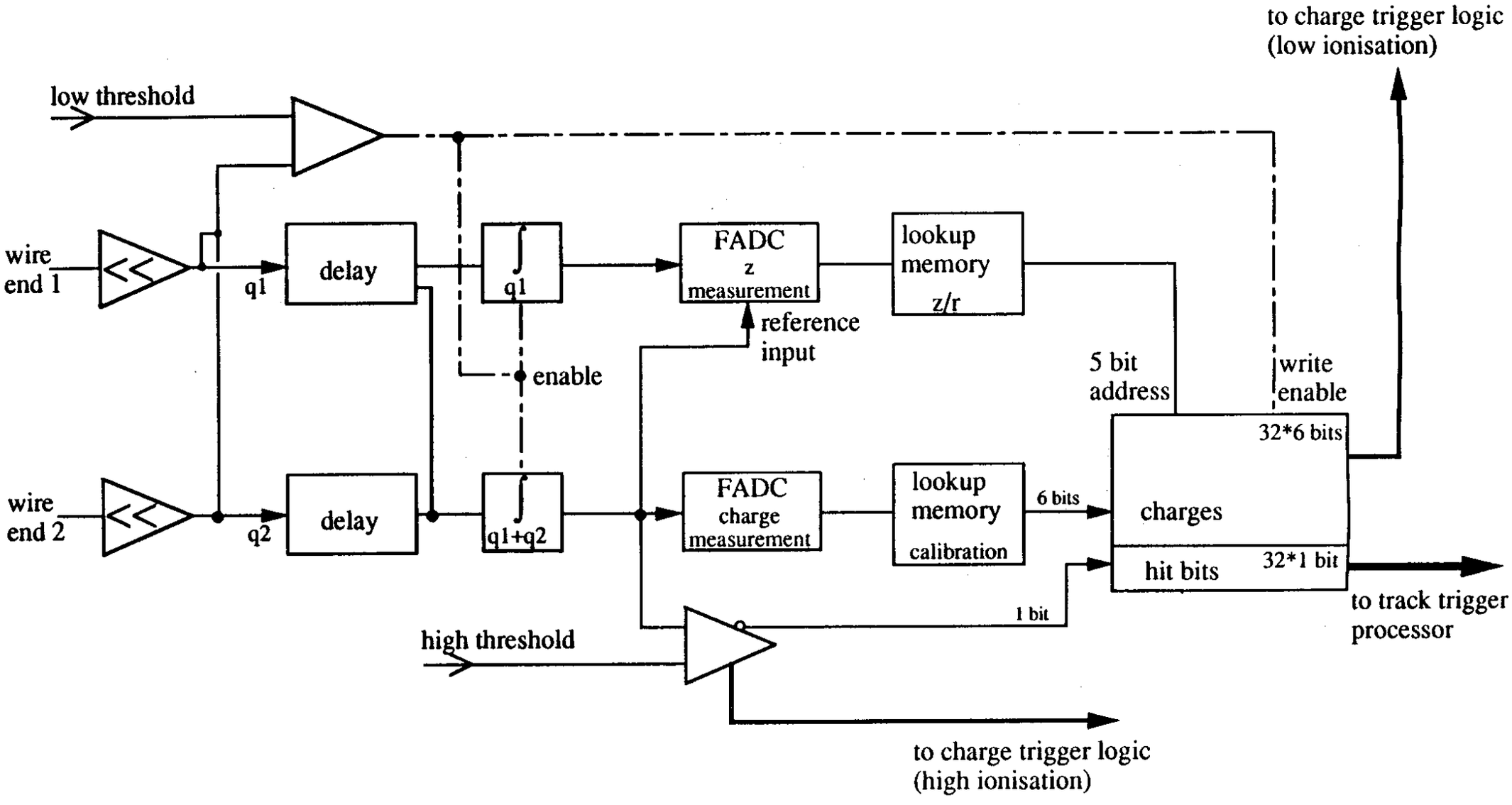
to charge trigger logic
(low ionisation)
low threshold
wire
end 1
q1
delay
q1
FADC
z
measurement
lookup
memory
z/r
reference
input
enable
5 bit
address
write
enable
32*6 bits
wire
end 2
q2
delay
q1+q2
FADC
charge
measurement
lookup
memory
calibration
6 bits
charges
hit bits
32*1 bit
1 bit
to track trigger
processor
high threshold
to charge trigger logic
(high ionisation)

Fig. 5

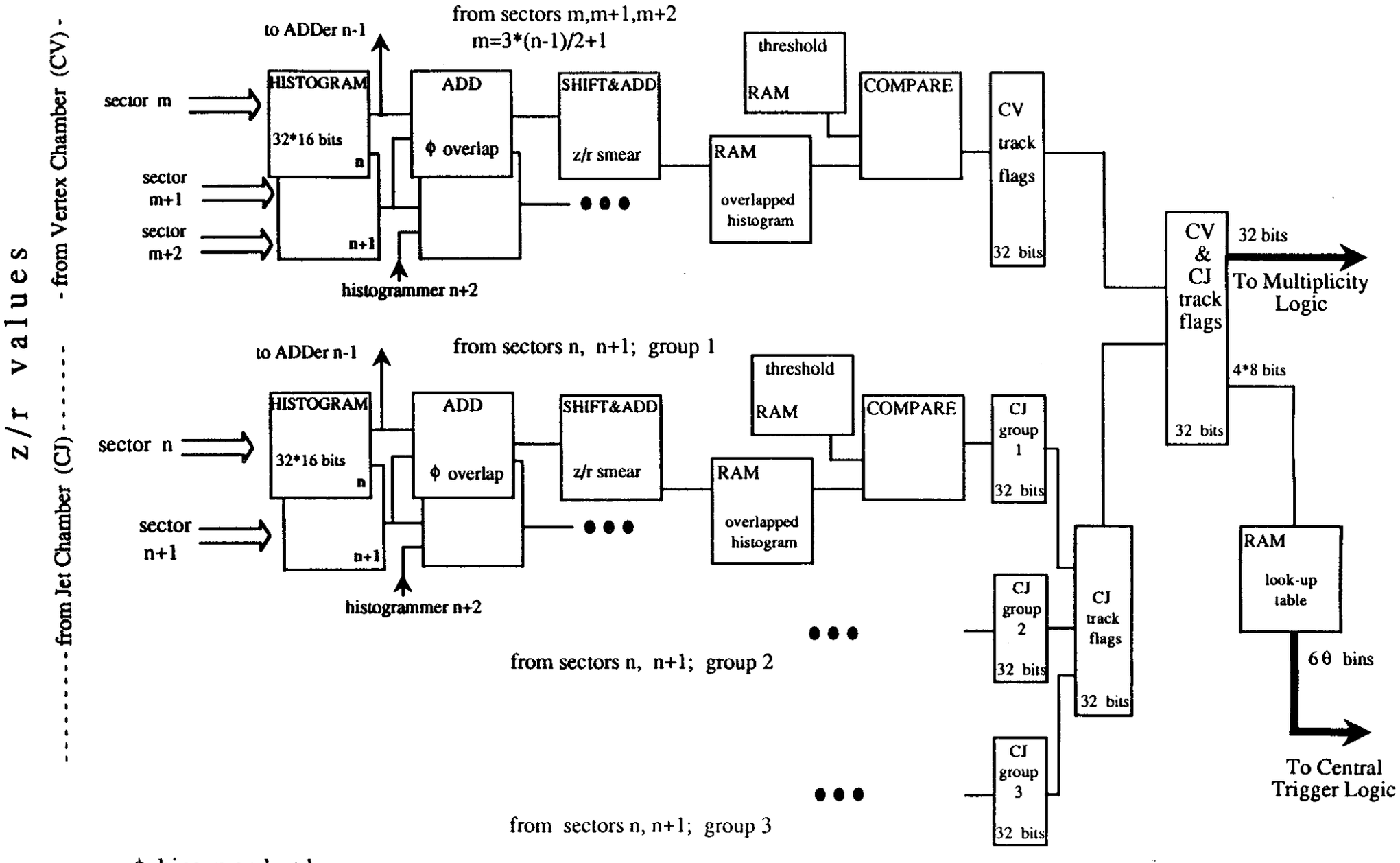
z/r values
- from Vertex Chamber (CV) -
- - - - - - - from Jet Chamber (CJ) - - - - - - -
from sectors m,m+1,m+2
m=3*(n-1)/2+1
to ADDer n-1
sector m
sector m+1
sector m+2
HISTOGRAM
32*16 bits
n
n+1
ADD
ϕ overlap
SHIFT&ADD
z/r smear
threshold
RAM
RAM
overlapped histogram
COMPARE
CV track flags
32 bits
histogrammer n+2
CV & CJ track flags
32 bits
32 bits
To Multiplicity Logic
4*8 bits
from sectors n, n+1; group 1
to ADDer n-1
sector n
sector n+1
HISTOGRAM
32*16 bits
ADD
ϕ overlap
SHIFT&ADD
z/r smear
threshold
RAM
RAM
overlapped histogram
COMPARE
CJ group 1
32 bits
histogrammer n+2
CJ group 2
32 bits
CJ track flags
32 bits
RAM
look-up table
6θ bins
To Central Trigger Logic
from sectors n, n+1; group 2
CJ group 3
32 bits
from sectors n, n+1; group 3
ϕ bins n and n+1
n = 1, 3, ... , 23

Fig. 6

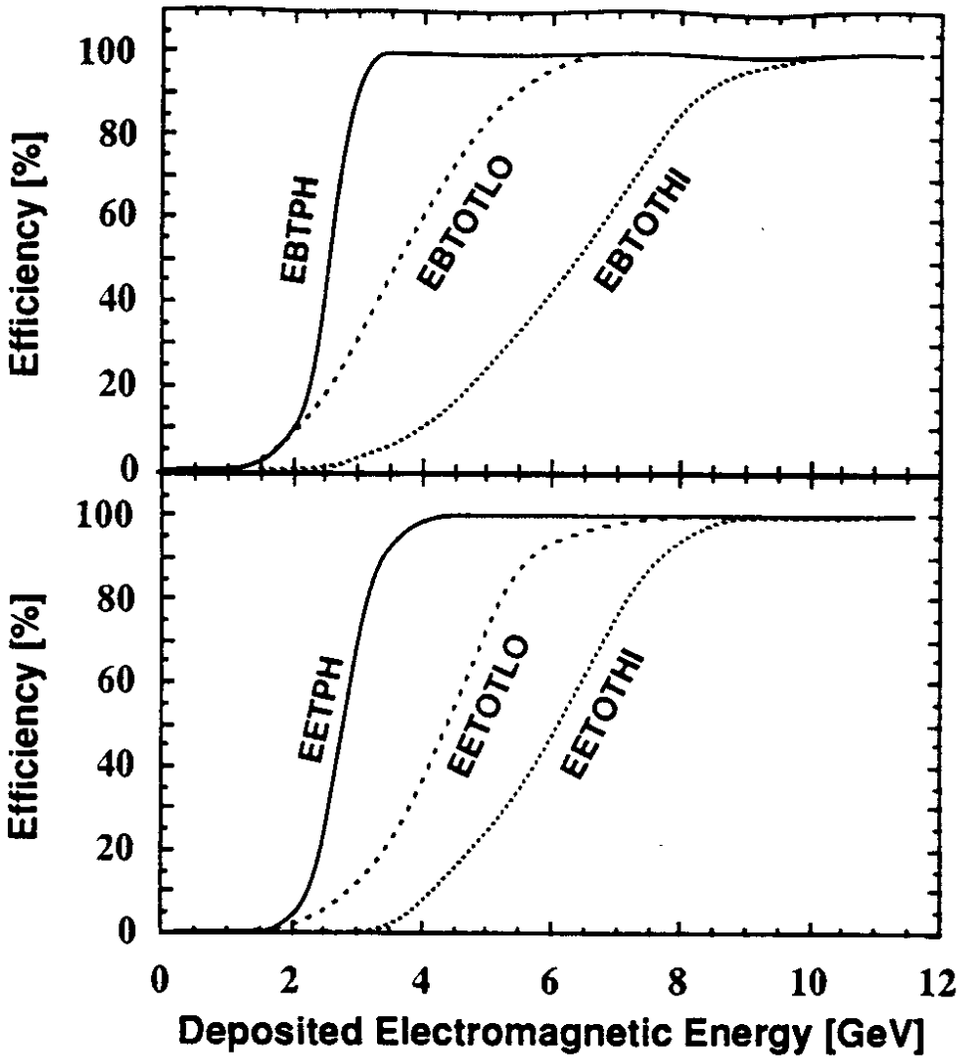
Efficiency [%]
100
80
60
40
20
0
EBTPH
EBTOTLO
EBTOTHI
Efficiency [%]
EETPH
EETOTLO
EETOTHI
0
2
4
6
8
10
12
Deposited Electromagnetic Energy [GeV]

Fig. 7

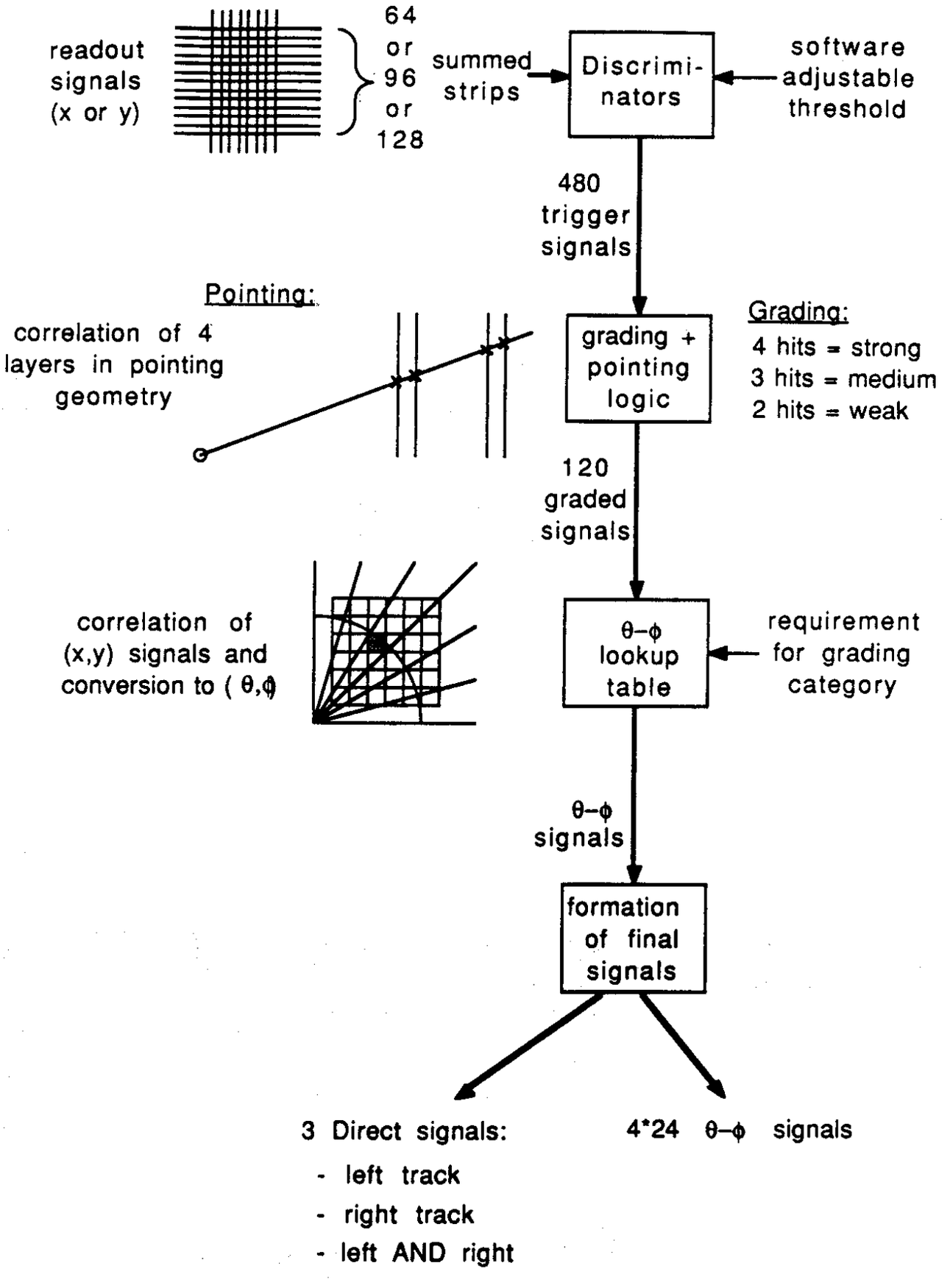
readout signals (x or y)
64 or 96 or 128
summed strips
Discrimi-nators
software adjustable threshold
480 trigger signals
Pointing:
correlation of 4 layers in pointing geometry
grading + pointing logic
Grading:
4 hits = strong
3 hits = medium
2 hits = weak
120 graded signals
correlation of (x,y) signals and conversion to (θ,ϕ)
θ–ϕ lookup table
requirement for grading category
θ–ϕ signals
formation of final signals
3 Direct signals:
- left track
- right track
- left AND right
4*24 θ–ϕ signals

Fig. 8

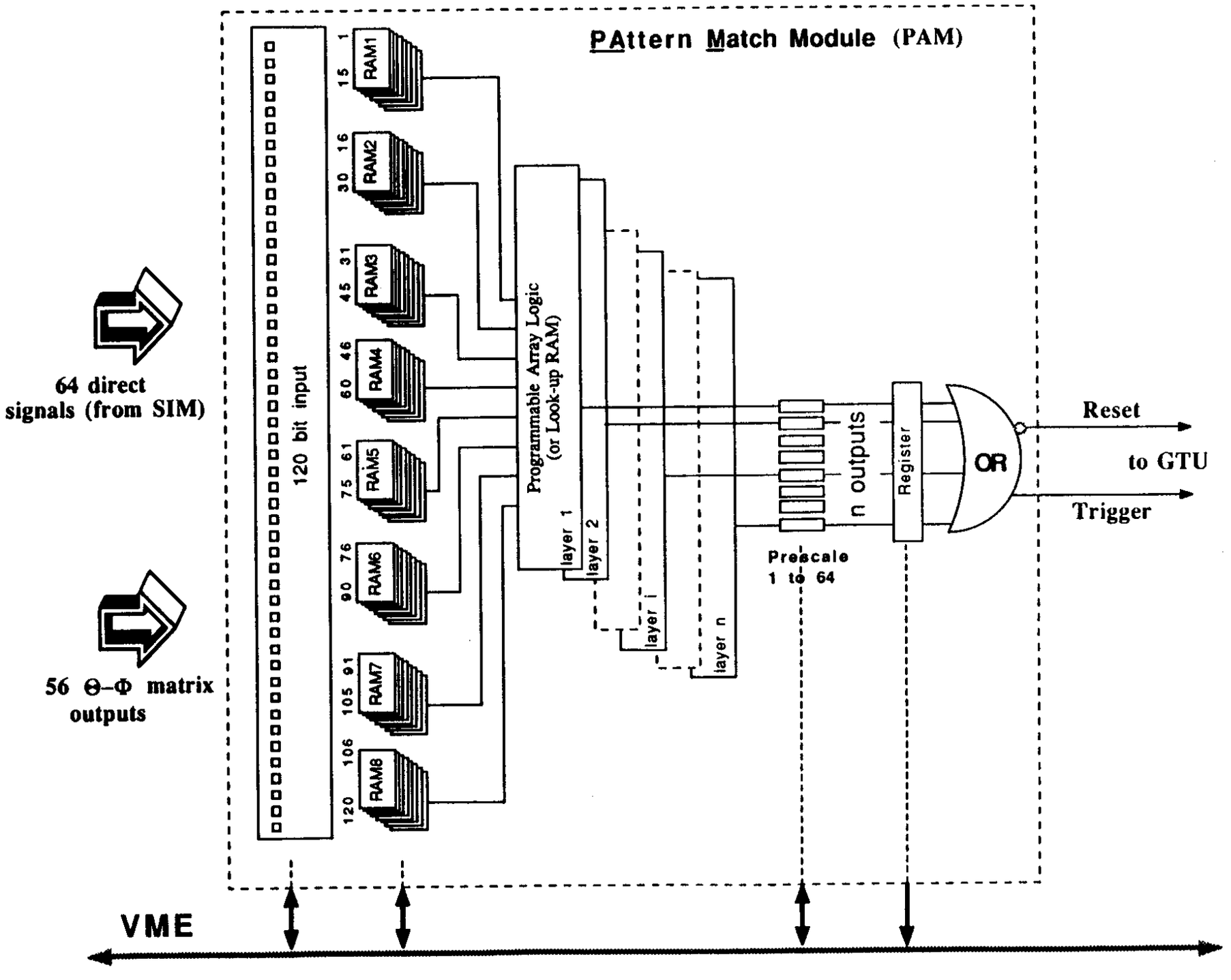

Fig. 9